Natural sea-salt emissions moderate the climate forcing of anthropogenic nitrate

Ying Chen[1,2,3,8,*], Yafang Cheng[2,*], Nan Ma[4,2,3,1], Chao Wei[3], Liang Ran[5], Ralf Wolke[1], Johannes Größ[1], Qiaoqiao Wang[4], Andrea Pozzer[6], Hugo A. C. Denier van der Gon[7], Gerald Spindler[1], Jos Lelieveld[6,9], Ina Tegen[1], Hang Su[3], Alfred Wiedensohler[1]

[1]Leibniz-Institute for Tropospheric Research, Leipzig, Germany
[2]Minerva Research Group, Max Planck Institute for Chemistry, Mainz, Germany
[3]Multiphase Chemistry Department, Max Planck Institute for Chemistry, Mainz, Germany
[4]Center for Pollution and Climate Change Research (APCC), Institute for Environmental and Climate Research, Jinan University, Guangzhou, China
[5]Key Laboratory of Middle Atmosphere and Global Environment Observation, Institute of Atmospheric Physics, Chinese Academy of Sciences, Beijing, China
[6]Atmospheric Chemistry Department, Max Planck Institute for Chemistry, Mainz, Germany
[7]TNO, Dept. of Climate, Air and Sustainability, Princetonlaan 6, Utrecht, the Netherlands
[8]Lancaster Environment Centre, Lancaster University, Lancaster, UK
[9]The Cyprus Institute, Nicosia, Cyprus

*Correspondence to: yafang.cheng@mpic.de (Y.F.C.); chen@tropos.de (Y.C.)

Abstract. Natural sea-salt aerosols, when interacting with anthropogenic emissions, can enhance the formation of particulate nitrate. This enhancement has been suggested to increase the direct radiative forcing of nitrate, called 'mass-enhancement effect'. Through a size-resolved dynamic mass transfer modelling approach, we show that interactions with sea-salt shift the nitrate from sub- to super-micron sized particles ('re-distribution effect'), and hence lower its efficiency for light extinction and reduce its lifetime. The re-distribution effect overwhelms the mass-enhancement effect and significantly moderates nitrate cooling; e.g., the nitrate associated aerosol optical depth can be reduced by 10-20% over European polluted regions during a typical sea-salt event, in contrast to an increase by ~10% when only accounting for the mass-enhancement effect. Global model simulations indicate significant re-distribution over coastal and offshore regions world-wide. Our study suggests a strong buffering by natural sea-salt aerosols that reduces the climate forcing of anthropogenic nitrate, which had been expected to dominate the aerosol cooling by the end of the century. Comprehensive considerations of this re-distribution effect foster better understandings of climate change and nitrogen deposition.

1. Introduction

Particulate nitrate (NO_3^-) is one of the most important anthropogenic aerosol components that exert a climate cooling effect (IPCC, 2013;Haywood and Schulz, 2007). On a global scale, its average direct radiative forcing (DRF) has been estimated to span over a relatively wide range from -0.08 to -0.19 W m^{-2} (Liao et al., 2004;Liao and Seinfeld, 2005;IPCC, 2013;Xu and Penner, 2012;Haywood and Schulz, 2007;Myhre et al., 2013;Forster et al., 2007;Adams et al., 2001;Bauer et al., 2007;Jacobson, 2001;Streets et al., 2013;van Dorland et al., 1997). It is projected to reach up to about -0.4 to -1.3 W m^{-2} and dominate the aerosol cooling by the end of the century (Adams et al., 2001;Bellouin et al., 2011;Hauglustaine et al., 2014). Although the gaseous precursors of nitrate, e.g., NOx (= NO + NO$_2$) and HNO$_3$, are mainly of anthropogenic origin, globally about 35-50% of the nitrate mass is associated with natural sea-salt aerosol (Xu and Penner, 2012;Myhre et al., 2006). This is because sea-salt aerosol can be transported over industrialized regions, interacts with anthropogenic precursors of nitrate and enhances the total nitrate column loading in the atmosphere through heterogeneous uptake of HNO$_3$ and its precursors (Liao et al., 2004;Liao and Seinfeld, 2005;Seinfeld and Pandis, 2006;Xu and Penner, 2012;Ravishankara, 1997;Lowe et al., 2015). Such sea-salt-induced nitrate mass increase is believed to strengthen the DRF and climate cooling of nitrate (Liao and Seinfeld, 2005), called the 'mass-enhancement effect'.

However, not only the mass concentration but also the particle mass size distribution (PMSD) are essential for evaluating the direct radiative forcing of nitrate (DRF$_{nitrate}$) (IPCC, 2013;Murphy et al., 1998;Kok et al., 2017). Besides leading to the increase of total nitrate mass, interactions with sea-salt aerosol also have a 're-distribution effect' on nitrate PMSD which shifts nitrate from sub- to super-micron sizes (e.g., Chen et al., 2016a, see also Fig. 1). Because sea-salt aerosol is mainly present as super-micron (coarse) particles (Murphy et al., 1998;O'Dowd et al., 1997;Ravishankara, 1997), chemical equilibrium favors the formation of thermodynamically stable sodium nitrate in the coarse mode, which inhibits the formation of semi-volatile ammonium nitrate in the sub-micron size (fine mode) through competitive consumption of gaseous precursors and change of gas-particle equilibrium (Chen et al., 2016a;Zaveri et al., 2008;Myhre et al., 2006). Compared to the fine particles, coarse particles have a significantly lower extinction efficiency in the visible part of the spectrum (IPCC, 2013;Murphy et al., 1998), the sea-salt-induced 're-distribution effect' thus tends to weaken DRF$_{nitrate}$, which counteracts the 'mass-enhancement effect'. The competition between these two effects will ultimately determine the net impact of sea-salt aerosol on anthropogenic DRF$_{nitrate}$. To

the best of our knowledge, this sea-salt-induced 're-distribution effect' is neglected in most global models, due to the computationally expensive calculations of fully dynamic mass transfer between size-resolved

65   particulate nitrate (Adams et al., 2001;Myhre et al., 2006); for more details see Supplementary Information Section S1.

To explore the competition between the sea-salt-induced 'mass-enhancement effect' and 're-distribution effect' and the impact of the 're-distribution' process on the nitrate cooling of climate, we conducted a series of sensitivity studies with and without sea-salt aerosol emission for a typical sea-salt event over Europe and

70   North America, using a regional atmospheric chemistry model (WRF-Chem) with a fully dynamic mass transfer approach (Zaveri et al., 2008); see 'Data & Methods' for details. A one-year simulation with the EMAC (ECHAM5/MESSy Atmospheric Chemistry) model is used to demonstrate the importance of the 're-distribution effect' on a global scale (Jöckel et al., 2010).

75   **2. Data & Methods**

2.1 Observations

The HOPE campaign (HD(CP)[2] Observational Prototype Experiment, Macke et al., 2017) at Melpitz, Germany, was carried out during 10-20 September 2013 at Melpitz (12.93°E, 51.53°N, 86 m a.s.l.). Melpitz represents the regional background of central Europe (Spindler et al., 2012), with flat surrounding

80   topography over an area of hundreds of square kilometers, ranging 100-250 m a.s.l.

Size-segregated measurements of particles composition were carried out on 13 September and 18 September, which represent the continental period and marine period, respectively (see back-trajectories in Fig. S1). A five-stage Berner impactor (Hauke, Austria, 0.05-0.14 μm, 0.14-0.42 μm, 0.42-1.2 μm, 1.2-3.5 μm, and 3.5-10 μm; Berner and Luerzer, 1980) was operated to segregate particles onto ring-like pre-baked

85   (350 °C) aluminium foils with a sampling period of 24 h (00:00-24:00, local time) for detailed chemical analyses (Spindler et al., 2012). The isokinetic inlet for particles with an aerosol dynamic diameter smaller than 10 μm was installed 6 meters above the ground. To compare with modelling results, we use the sum of the particle mass at stage 1-3 ($PM_{1.2}$, aerosol dynamic diameter smaller than 1.2 μm) to represent fine mode particles and the sum of the mass at stages 4-5 ($PM_{1.2-10}$, aerosol dynamic diameter smaller between 1.2 and

90   10 μm) to represent coarse mode particles. The gravimetric mass of the pre-heated aluminium foils was

weighted respectively before and after the sampling process, by a microbalance (UMT-2, Mettler-Toledo, Switzerland). Before each weighting, the aluminium foils were equilibrated for at least 72 hours in a strictly controlled environment with a temperature of 20±1 $^\circ$C and a relative humidity of 50±5%. After an aqueous extraction of foil aliquots, the main water-soluble cations (Na$^+$, NH$_4^+$, K$^+$, Mg^{2+} and Ca^{2+}) were quantified by standard ion chromatography (Neusüß et al., 2000). Likewise, capillary electrophoresis (Neusüß et al., 2000) was carried out to quantify the anions (NO$_3^-$, SO$_4^{2-}$ and Cl$^-$). A carbon analyzer (Behr Labor-Technik, Germany) was used to separate and measure the sampled organic and elemental carbon with a two-step thermographic method (modified VDI method 2465 part-2, Spindler et al., 2012). Organic carbon was vaporized at 650 $^\circ$C for 8 minutes under N$_2$ and catalytically converted to CO$_2$; the remaining elemental carbon was combusted for another 8 minutes with O$_2$ at 650 $^\circ$C. Generated CO$_2$ was then quantitatively determined using a non-dispersive infrared detector.

2.2 Model description

We performed regional model simulations with the 'online coupled' air quality model Weather Research and Forecasting/Chemistry model (WRF-Chem V3.5.1, Grell et al., 2005). WRF-Chem enables more detailed investigation of aerosol-radiation interaction over specific regions at higher horizontal resolution compared with global models, and has been broadly used for investigating aerosol radiative forcing in previous studies (e.g., Archer-Nicholls et al., 2019;Fast et al., 2006;Saide et al., 2012;Gao et al., 2018;Yao et al., 2017;Huang et al., 2015). To investigate the impact of 're-distribution effect' on PMSD and climate effect of nitrate, the fully dynamic aerosol module MOSAIC (Zaveri et al., 2008) was utilized with eight discrete size bins (39-78 nm, 78-156 nm, 156-312 nm, 312-625 nm, 625-1250 nm, 1.25-2.5 μm, 2.5-5 μm, 5-10 μm; see also Fig. 2), with the online coupled CBMZ (Carbon-Bond Mechanism version Z) gas chemistry scheme (Zaveri and Peters, 1999). In MOSAIC, NaCl reacts irreversibly with nitric acid with its equilibrium surface vapor pressure of zero; and a gas-particle partitioning approach ASTEM (Adaptive Step Time-Split Euler Method) is coupled with a thermodynamic module (MESA-MTEM, Multicomponent Equilibrium Solver for Aerosols – Multicomponent Taylor Expansion Method) to dynamically calculate the equilibrium vapor pressure and condensation rate of semi-volatile ammonium nitrate, details are given in the section 4 of Zaveri et al. (2008). We note that heterogeneous hydrolysis of N$_2$O$_5$ with NaCl is an important chemical pathway of particulate nitrate in coarse mode during nighttime (Bertram and Thornton, 2009;

120 Archer-Nicholls et al., 2014). This process may enhance the 're-distribution effect', however it is not considered in this study. The sea-salt emissions computed with the modified Gong scheme (Gong, 2003) were reduced to 10% in the 'Case_SeasaltOn', because a previous study (Chen et al., 2016a) has shown that the original Gong scheme overestimates the sea-salt mass concentrations by a factor of ~10 over the coastal regions of Europe using WRF-Chem model. We note that although the mass of coarse sea-salt particles is

125 certainly overestimated, it might not necessarily indicate overestimation in fine sea-salt particles related to their minor contribution to the total mass. The sea-salt emission was turned off in the 'Case_SeasaltOff' simulation. We calculate the DRF and aerosol optical depth of anthropogenic nitrate at the top of the atmosphere for both sea-salt emission cases, based on the difference in the net incoming radiative flux with and without the anthropogenically emitted gas phase precursor NOx (IPCC, 2013;Xu and Penner, 2012).

130 Only the model results during daytime (07:00-16:00, local time) and under clear-sky condition (cloud optical depth equals to zero) were used for the analyses of DRF in this study.

WRF-Chem calculated aerosol optical depth (AOD) and direct radiative effect of total aerosols based on the internal mixture assumption taking the hygroscopicity into account. In order to calculate the light extinction coefficient and optical depth for individual aerosol species, we performed the following off-line

135 calculation. The AOD of each species is calculated by integrating light extinction coefficient (σ_{ex}) over all vertical layers. The σ_{ex} of sea-salt (NaCl) and particulate nitrate were calculated with Mie theory, based on their PMSD. Different from the WRF-Chem calculation of total aerosol AOD, external mixture was assumed for nitrate and sea-salt particles when calculating their respective contributions on σ_{ex} or AOD. Hygroscopic growth was also considered, following the κ-Köhler theory (Köhler, 1936;Petters and Kreidenweis, 2007).

140

2.3 European simulation

The European simulations focus on the HOPE-Melpitz campaign period of 10-20 September 2013, during which a sea-salt event that influenced most part of Europe was captured. The simulations are defined by two nested domains with horizontal resolutions of 54 km and 18 km respectively, and 39 vertical layers

145 with model top at 50 hPa. The coarse domain (D01) covers the North Sea, the European continent and the northern part of Africa; the inner domain (D02) covers most of the North Sea and the European continent (Fig. S2). The European anthropogenic emission inventories are provided by TNO (www.tno.nl) from the AQMEII project (Air Quality Model Evaluation International Initiative) for PM$_{2.5}$, PM$_{2.5-10}$, NOx, SO$_2$, CO,

NH$_3$, and non-methane volatile organic compounds (Pouliot et al., 2012;Chen et al., 2018b), and from the EUCAARI project (European Integrated project on Aerosol, Cloud, Climate, and Air Quality Interactions) for particulate organic carbon and elemental carbon (Kulmala et al., 2011). The inventories are with a spatial resolution of 1/8º × 1/16º longitude-latitude. We excluded the point source emissions of elemental carbon in EUCAARI inventory over Germany, since a previous study (Chen et al., 2016b) reported large uncertainty of them. More details about emissions, meteorological and chemical initial/boundary conditions can be found in the Supplementary Information Section S2. Detailed information about the model configuration is given in Table 1.

In the European 'Case_SeasaltOn' simulation (with sea-salt emission), modelled [Na$^+$] showed good agreement with measurements over coastal regions from European Monitoring and Evaluation Programme (EMEP, http://www.emep.int), with a factor (and correlation coefficient) of 0.85 (0.67), 1.16 (0.80) and 0.83 (0.87) for Bilthoven, Kollumerwaard and Vredepeel (Fig. S3), respectively. Compared with ground-based measurements at Melpitz and radio-sounding measurements across Europe, the meteorological conditions were well captured by the model (Chen et al., 2016a). Vertical structures of potential temperature and wind speed were realistically reproduced, with correlation coefficients between simulation and measurement results of ~0.9 over coastal, German low land (Melpitz) and northern Polish regions (Chen et al., 2016a). In line with previous studies (Xu and Penner, 2012;Li et al., 2013), the modelled AOD agreed reasonably well with the AERONET observations (AErosol RObotic NETwork, http://aeronet.gsfc.nasa.gov). The spatial distribution of AOD can be generally captured by the model (R=0.64), although model may overestimate AOD by a geometric mean bias of 70% (see Supplementary Information Section S3 for details).

2.4 North America and global simulations

To investigate the significance of the 're-distribution effect' in a broader spatial scale, we also conducted WRF-Chem simulation over North America, where high concentrations of nitrate were usually observed. We focus on the period of 10-17 January 2015, when strong continental outflow interacted with marine air masses over the Gulf of Mexico. The North American domain covers the US, the Gulf of Mexico and parts of Pacific and Atlantic oceans, with a horizontal resolution of 36 km. In addition, a one-year simulation with global model (EMAC) was carried out for analysis of the potential impact of 're-distribution effect' on a global scale. Although the fully dynamic mass transfer between particle sizes is not considered

in EMAC (four size modes rather than eight size bins as applied in the WRF-Chem model), we adopt a parameterization derived from WRF-Chem simulations to estimate the potential impact (details given in section 3.5). More details of EMAC model and its aerosol module are described in our previous work (Pozzer et al., 2012;Klingmüller et al., 2014;Pringle et al., 2010). The global simulation was run at T106L31 resolution, corresponding to a quadratic Gaussian grid of approximately 1.1º × 1.1º (in latitude and longitude) and with 31 levels in the troposphere. The global emission inventory EDGAR (V4.3, 2010, http://edgar.jrc.ec.europa.eu) was used in the North American and global simulations.

3. Results and Discussion

3.1 Sea-salt-induced 're-distribution effect'

Marine air masses frequently, ~up to 90% of the days in a year, influence Central Europe (Birmili et al., 2001). The interaction between anthropogenic pollutants and sea-salt aerosol commonly happens in the atmosphere. In this study, we performed a series of numerical sensitivity experiments during a typical *sea-salt transport event* from 10 to 20 September 2013 during the HOPE-Melpitz campaign. During the campaign, Central Europe was dominated by continental air masses before 15 September. Subsequently marine air masses started travelling over land on 17 September, and sea-salt aerosol originating from the North Sea and the Baltic Sea was transported to northern Poland and dominated Central Europe on 19 September (Fig. 3). Sea-salt is emitted into the marine planetary boundary layer (PBL) with mass concentration dominated by coarse particles, usually with a short lifetime and a limited transport range. Previous studies showed that the special PBL thermodynamic structure over coastal regions (Ding et al., 2004) can bring sea-salt from the marine PBL to the continental free troposphere, therefore prolonging its lifetime and favoring long-range transport (see the figure 11 of Chen et al. 2016a). Afterwards, the sea-salt aloft could be mixed down to surface layer by the fully developed PBL (Chen et al., 2009;Chen et al., 2016a) and interact with anthropogenic nitrate. Therefore, this transport mechanism broadens the sea-salt-induced 're-distribution effect' on nitrate to a larger spatial scale.

As shown in Fig. 4a and 4b, the 'Case_SeasaltOn' simulation successfully reproduces the 're-distribution effect' of nitrate when the dominating air mass changed from a continental to marine type at the Central Europe background site Melpitz. Measurements and model results both show an ~10 times increase of sodium concentration ([Na^+], indicator of sea-salt aerosol) in the coarse mode when marine air masses

approached (Fig. S4). While the nitrate mass fraction in the coarse mode was enhanced by a factor of ~5.5, its concentration ($[NO_3^-]$) in the fine mode was lowered by ~20% (Fig. 4b). A clear re-distribution of particulate nitrate from fine to coarse mode is found when introducing sea-salt in the 'Case_SeasaltOn', with negligible changes in other particulate species except sea-salt (Fig. 2). Conversely, without introducing sea-salt aerosol, the 'Case_SeasaltOff' did not capture the 're-distribution effect', and the nitrate mass in the fine mode (~97%) dominated in both continental and marine air masses (Fig. 4c).

3.2 Moderation of nitrate cooling by the 're-distribution effect'

Figure 5 shows the strong impact of the 're-distribution effect' on nitrate cooling when marine air mass transported further inland and predominated over Europe on 19 September. Although sea-salt aerosol leads to an overall enhancement of nitrate column loading (~1 mg m^{-2}, Fig. S5) compared to the 'Case_SeasaltOff', the nitrate associated aerosol optical depth ($AOD_{nitrate}$) decreases significantly over the relatively polluted continental regions (Fig. 5a), leading to a strongly weakened cooling effect of nitrate in those regions (positive change in $DRF_{nitrate}$ in Fig. 5b). We find that the regions of reduced $AOD_{nitrate}$ co-locate with the regions of reduced fine mode $[NO_3^-]$ (bluish colored areas in Fig. 5a and 5c). Over a large area of the European continent, the 're-distribution effect' shifts the nitrate PMSD from the fine to the coarse mode (Fig. 5c, 5d), resulting in much less efficient light scattering of nitrate aerosol with a reduced cooling effect. The box with a solid black frame in Fig. 5 marks a region in northern Poland, where sea-salt aerosol strongly interacted with anthropogenic precursors of nitrate during the studied sea-salt event. In this region, 're-distribution effect' leads to a decrease of column nitrate loading in the fine mode by ~2.9 mg m^{-2} (Fig. 5c) accompanied by an increase of ~3.7 mg m^{-2} in the coarse mode due to the 'mass-enhancement effect' (Fig. 5d). Consequently, the anthropogenic $AOD_{nitrate}$ is significantly reduced by up to ~30% with an average reduction of ~22% (~0.05 in absolute AOD value, Fig. 5a), despite of a ~0.8 mg m^{-2} net increase in total nitrate loading. This results in a 5-70% reduction of nitrate cooling, on average by ~26% (Fig. 5b). Our results demonstrate that the sea-salt-induced 're-distribution effect' overwhelms the 'mass-enhancement effect' over polluted regions, thus moderating the anthropogenic nitrate cooling.

The resulting decrease of nitrate cooling is non-linear with respect to the sea-salt aerosol loading due to the competition between sea-salt-induced 'mass-enhancement effect' and 're-distribution effect'. To investigate the net impact of this competition, we performed a series of sensitivity simulations with different

sea-salt aerosol emission scaling factors (0, 0.5, 1, 2, 3, 4, 5, 6, 8, and 10, the ones with scaling factors of 0 and 1 being our 'Case_SeasaltOff' and 'Case_SeasaltOn', respectively). As a surrogate of aerosol DRF, the AOD of nitrate and sea-salt aerosol was calculated offline based on the simulated PMSD (see 'Data & Methods'). Over the region in northern Poland (box with solid frame in Fig. 5), total $[NO_3^-]$ (green dashed line in Fig. 6a) increased continuously as a function of $[Na^+]$, which is in line with previous estimates and clearly shows the 'mass-enhancement effect' (Liao and Seinfeld, 2005). However, the 're-distribution effect' overwhelms the 'mass-enhancement effect' in this region, and the $AOD_{nitrate}$ drops significantly by ~29% (red solid line in Fig. 6a) when the scaling factor of sea-salt aerosol is 1 ('Case_SeasaltOn'), Noting that this is slightly higher than the average ~22% from the on-line calculation, due to the difference in aerosol mixing state, i.e., internal mixing of aerosol compositions in the on-line calculation; and external mixing in the offline calculation. The reduction of $AOD_{nitrate}$ reaches a maximum of ~50% (~0.09 in absolute AOD value) when $[Na^+]$ is ~2.5 μg m^{-3} or higher, which level of sea-salt aerosol has been often observed in Central Europe (Fig. 6c, Gustafsson and Franzén, 2000;Neumann et al., 2016;Gantt et al., 2015). A similar net reduction of $AOD_{nitrate}$ is also found for Central Europe (marked in Fig. 3), where the overall moderation is ~13% compared to the 'Case_SeasaltOff' (Fig. S6a). To further demonstrate the influence of the 're-distribution effect' on nitrate cooling, we calculate the $\Delta AOD_{nitrate}$ by re-allocating nitrate mass into different size bins according to the normalized nitrate PMSD simulated in the 'Case_SeasaltOff', i.e., by neglecting the 're-distribution effect' ($\Delta AOD^*_{nitrate,}$ pink dashed line in Fig. 6a). A distinct opposite trend, of increasing $AOD^*_{nitrate}$ with increasing $[NO_3^-]$ (green dashed line), would result when the 're-distribution effect' was neglected. For example, instead of a decrease by 29%, the $AOD^*_{nitrate}$ over the region of northern Poland increases by ~8% from the 'Case_SeasaltOff' to the 'Case_SeasaltOn'.

It is noteworthy that the increase rate of $[NO_3^-]$ decreases as $[Na^+]$ further increases. There is even a slight decrease of $[NO_3^-]$ when $[Na^+]$ exceeds ~5 μg m^{-3} (Fig. 6a). This is mostly due to the consumption of nitrate precursor and stronger deposition of particulate nitrate by 're-distribution' toward larger particles sizes and, thus, shorter lifetimes. The lifetime of nitrate particles can be shortened from about a week to one day by shifting from the fine to the coarse mode (Croft et al., 2014;Chen et al., 2016b) further moderate nitrate cooling effect. Moreover, coarse mode nitrate associated with highly hygroscopic sea-salt enhances its water uptake (Chen et al., 2018a) and cloud condensation nuclei activation (Xu and Penner, 2012;Wang and Chen, 2019), fastening its deposition and scavenge rate. Itahashi et al. (2016) reported that oxidized

nitrogen deposition can be enhanced by 1.6-2.2 times over ocean regions in East Asia by including sea-salt associated nitrate. Liao and Seinfeld (2005) implied a similar enhancement for sea-salt/dust associated sulfate deposition, which resulted in a decrease in sulfate concentrations in the downwind regions. Our study implies the enhancement of nitrate deposition. As one can see in Fig. 6a, nitrate concentration (green dashed line) firstly increases with increasing sea-salt and then slightly declines when the amount sea-salt (represented by sodium) exceeds a certain level. An inflection point is observed when sodium concentration approached 5.5 μg m^{-3} (sea-salt emission factor = 8), the nitrate starts to decrease as sodium further increases (sea-salt emission factor = 10). The enhancement of nitrate deposition should be the reason of this phenomenon. To demonstrate this, we conducted a sensitivity simulation with aerosol dry deposition turned off. We found that nitrate concentration kept increasing from 10.91 to 11.02 μg m^{-3} when sea-salt emission factors increased from 8 to 10, instead of showing a decreasing trend as in the simulations with aerosol dry deposition turned on. This indicates an enhanced deposition of nitrate by interaction with sea-salt which shortens nitrate lifetime and can further reduce nitrate cooling.

3.3 Competition between 're-distribution effect' and 'mass-enhancement effect'.

As a result of competition between the sea-salt-induced 're-distribution effect' and 'mass-enhancement effect', clear spatial inhomogeneity can be found in Fig. 5. The 're-distribution effect' decreases AOD$_{nitrate}$ over the polluted continental regions; while the 'mass-enhancement effect' increases AOD$_{nitrate}$ mostly over marine areas (Fig. 5a), although the absolute enhancement is rather small due to the low [NO$_3^-$] in this environment. For example, over the Mediterranean Sea (marked by the box with a dashed black frame in Fig. 5), the AOD$_{nitrate}$ increases by ~0.01 and the cooling effect of nitrate is amplified by ~0.54 W m^{-2} (negligible without introducing sea-salt aerosol). Sensitivity study also shows a monotonic increase of AOD$_{nitrate}$ with [Na$^+$] over the Mediterranean Sea (Fig. 6b), indicating a dominant role of the 'mass-enhancement effect' over regions with limited anthropogenic influence.

Thus, abundant sea-salt aerosol and pre-existing fine mode nitrate (as if no sea-salt aerosol influence in the 'Case_SeasaltOff') favor an efficient 're-distribution effect' that reduces AOD$_{nitrate}$ and moderates nitrate cooling. To compare the relative importance of the sea-salt-induced 're-distribution effect' and 'mass-enhancement effect' on anthropogenic nitrate cooling, we conducted statistical analysis of the molar ratio between fine nitrate in the 'Case_SeasaltOff' and total sodium in the 'Case_SeasaltOn' (RNS = [NO$_3^-$]/[Na$^+$]

in mol mol^{-1}) with relation to the percentage change of nitrate AOD (surrogate of DRF$_{nitrate}$) between the two cases, i.e., (AOD$_{nitrate\ Case\_SeasaltOn}$ − AOD$_{nitrate\ Case\_SeasaltOff}$)/AOD$_{nitrate\ Case\_SeasaltOn}$. We found that the 're-distribution effect' tends to be strong enough to overwhelm the 'mass-enhancement effect' when the RNS value is in the range of about 1 to 30, corresponding to ~70% of the data points in the European domain, as detailed in Supplementary Information (Fig. 7c and Section S4). Note that only the surface concentrations were used for calculating the RNS, because fine mode ammonium nitrate is mostly limited in the surface layer because emissions of NH$_3$ are in surface layer. The sea-salt (or sodium) aloft during transport process (as discussed in section 3.1) did not exert the 're-distribution effect' before being mixed down to surface layer, and should not be included in the analysis. Therefore, we carried out a statistical analysis with surface nitrate and sodium concentrations, to draw a more robust conclusion. When the 're-distribution effect' is sufficiently strong, the net reduction of AOD$_{nitrate}$ may even counteract the AOD enhancement contributed by the additional sea-salt aerosol loading and lead to an overall reduction of total AOD in many regions in Europe (Supplementary Information Fig. S6b and Section S5).

3.4 The 're-distribution effect' over Europe

Due to the frequent interactions between sea-salt aerosol and polluted air masses (Myhre et al., 2006;Xu and Penner, 2012), the moderation of nitrate cooling is expected to be common over Europe, where the lower atmosphere is characterized by RNS values between 1 and 30 (Fig. 7). As discussed above (Fig. 6a and Fig. S6), considerable moderation is expected over inland and Central Europe, where [Na$^+$] > 2.5 μg m^{-3} is observed frequently (Gustafsson and Franzén, 2000, also see Fig. 6c). Such moderation could be even more relevant over coastal and continental outflow regions of North America and South/East Asia (discussed in the next section), where high loadings of nitrate were observed and found to be significantly associated with sea-salt aerosol (30-90% of total nitrate) (Xu and Penner, 2012).

To quantify the possible overestimation of nitrate radiative forcing when only the sea-salt-induced 'mass-enhancement effect' was treated but not the 're-distribution effect', similar statistical analysis (Fig. 7a) is conducted for the percentage change of nitrate AOD between the AOD$_{nitrate}$ in the 'Case_SeasaltOn' and the corresponding AOD$^*_{nitrate}$, i.e. (AOD$_{nitrate}$ − AOD$^*_{nitrate}$)/AOD$_{nitrate}$. As described before, AOD$_{nitrate}$ stands for the case where both 'mass-enhancement' and 're-distribution' effects have been accounted for the 'Case_SeasaltOn', while only the 'mass-enhancement effect' is accounted for AOD$^*_{nitrate}$. Fig. 7b shows that

the $AOD^*_{nitrate}$ could increase by 5-30% when introducing sea-salt and only the 'mass-enhancement effect' is considered. Conversely, the statistics show that the 're-distribution effect' tends to significantly reduce the nitrate AOD by 10-20% when there is abundant sea-salt interacting with anthropogenic nitrate (RNS < ~30, Fig. 7a). Note that this estimation of percentage reduction in $AOD_{nitrate}$ is robust (may be slightly conservative), despite of the overestimation of particulate nitrate over Europe (Supplementary Information Section S6). The uncertainty in deposition parameterizations could be one reason of this overestimation, as suggested by the overestimation of sea-salt particles as well (Chen et al., 2016a) and the underestimation of nitrogen deposition over Europe in many models (Vivanco et al., 2017). The upper limit of our result is comparable to a previous estimate of 25% reduction of $AOD_{nitrate}$ by sea-salt aerosol on a global scale by Myhre et al. (2006). They evaluated a similar 're-distribution effect' of sea-salt aerosol. But the simplifications of the mass transfer between fine and coarse modes may lead to overestimation of the reduction (Supplementary Information Section S1). The 're-distribution effect' becomes rather weak (limited within 10%) as RNS further increased (RNS > ~30) when marine air masses are transported further inland.

3.5 The 're-distribution effect' over North America and on a global scale

An additional simulation over North America confirms our findings. Similar as over Europe, the sea-salt-induced 're-distribution effect' predominates and reduces $AOD_{nitrate}$ over industrialized and outflow regions of the North America domain (Fig. 8). Generally, similar reduction of $AOD_{nitrate}$ is found over North America due to the sea-salt-induced 're-distribution effect'. A monotonous decrease (increase) of column fine (coarse) nitrate loading is observed all over North America and oceanic regions (Fig. 8c and Fig. 8d). This sea-salt-induced 're-distribution effect' overwhelms the 'mass-enhancement effect' over most regions and, thus, reduces $AOD_{nitrate}$ (Fig. 8a) and cooling effect of nitrate especially over the Gulf of Mexico (Fig. 8b), although the total nitrate column loading increases significantly (Fig. S7). This is because the high concentration of nitrate in the continental outflow from North and Central America strongly interacts with sea-salt over the Gulf (Xu and Penner, 2012).

The statistical analysis of the 're-distribution effect' over North America (Fig. 9a) shows a similar pattern as over Europe (Fig. 7a), and a first-order approximation ($R^2 > 90\%$) is derived from the European and North American results of WRF-Chem model to parameterize the relationship between RNS and the changes of $AOD_{nitrate}$ associated with the 're-distribution effect' (Fig. 9b). In general, the impact of the 're-

distribution effect' on $AOD_{nitrate}$ decreases as RNS increases. Only considering the 'mass-enhancement effect' but ignoring the 're-distribution effect' may lead to an overestimation of $AOD_{nitrate}$ by about 20% when RNS < 1, by about 10-20% when $1 \leq RNS \leq 30$ and by less than ~10% when RNS > 30.

On a global scale, the potential influence of the 're-distribution effect' on $AOD_{nitrate}$ is estimated by using the above first-order approximation combined with a one-year RNS simulation with the EMAC (Klingmüller et al., 2014;Pringle et al., 2010) chemistry-climate model (Fig. 10). The global distributions of percentage changes of $AOD_{nitrate}$ and surface nitrate concentration are given in Fig. S8. In line with the WRF-Chem results, a significant 're-distribution effect' is expected over North America and Europe, especially over the coastal regions with high nitrate loading and RNS values around 1 (Fig. 10b). As shown in Fig. 10c, the impact over Europe is stronger than over North America. The oceanic influence dominates over western Europe whereas over North America the predominantly more continental air masses (Kottek et al., 2006) may be a possible reason of this. It leads to less interactions of sea-salt with anthropogenic nitrate in North America, and more significant reduction of $AOD_{nitrate}$ over Europe. This result is consistent with a previous study (Myhre et al., 2006). Nevertheless, it is still possible that sea-salt is transported (May et al., 2018) further inland over North America and impacts $AOD_{nitrate}$ there. The coastal and offshore regions of Asia with $1 \leq RNS \leq 30$ may experience strong reductions of $AOD_{nitrate}$, where the 're-distribution effect' is expected to overwhelm the 'mass-enhancement effect', such as coastal and outflow regions of China. The influence of sea-salt aerosol becomes negligible over inland Asia where marine air mass influence is small (RNS > 30). For the open sea regions with RNS < 0.01 (white background), nitrate climate effect is not important, due to very limited nitrate loading contributing to $AOD_{nitrate}$ (Fig. 10a).

4. Summary and Discussion

The interaction between natural sea-salt aerosols and anthropogenic nitrate leads to the 're-distribution effect', which can shift the particulate nitrate from sub- to super-micron sizes. This effect lowers its mass light extinction efficiency and shorten its lifetime. This 're-distribution effect' can significantly moderate nitrate cooling.

The interaction between natural sea-salt aerosols and anthropogenic nitrate happens frequently over Europe (up to 90% of the days in a year). We performed a series of sensitivity studies during a typical sea-salt event over Europe, using WRF-Chem model with fully dynamic aerosol mass transfer treatment online-

coupled. The 're-distribution effect' of nitrate is observed by field measurements and well captured by the 'Case_SeasaltOn' simulation. Over the highly polluted northern Poland region, our sensitivity modelling results show that the 're-distribution effect' can reduce $AOD_{nitrate}$ by about 20-30%, or even up to ~50% when the sea-salt event is sufficiently strong. Conversely, if we only consider the increase of nitrate mass by introducing sea-salt ('mass-enhancement effect') and ignore the 're-distribution effect', nitrate AOD could increase by ~8% or even up to ~30% in a strong sea-salt event. We propose a single parameter, RNS ($[NO_3^-]/[Na^+]$ in mol mol^{-1}), to describe the competition between sea-salt-induced 're-distribution effect' and 'mass-enhancement effect'. In general, (1) the sea-salt-induced 'mass-enhancement effect' is dominant over oceanic regions and tends to increase $AOD_{nitrate}$; the dominance of 'mass-enhancement effect' could take place when RNS is lower than 1; (2) the sea-salt-induced 're-distribution effect' on nitrate PMSD can decrease $AOD_{nitrate}$ by about 10-20% and overwhelm the 'mass-enhancement effect' resulting in a net reduction of $AOD_{nitrate}$; this could take place when RNS is in the range between 1 and 30; and (3) the influence of sea-salt aerosol is not significant when RNS is higher than 30. These findings are further confirmed by the sensitivity simulations over North America. The impact of 're-distribution effect' on a global scale is estimated using global simulation of RNS. Significant 're-distribution effect' is expected over Europe, the Gulf of Mexico, Eastern Asia, coastal and offshore regions world-wide, may resulting in reduction of $AOD_{nitrate}$ by about 10-20%. This study demonstrates the suppression of AOD and DRF of particulate nitrate by the 're-distribution effect'. In addition, the 're-distribution effect' may also reduce the number of cloud condensation nuclei (CCN) by lowering the nitrate concentration in fine particles which are the main contributors to CCN number. The hygroscopicity of coarse sea-salt particles could also be reduced by associating with nitrate, which might suppress cloud droplet activation (Xu and Penner, 2012). Further studies are needed to investigate the influences of 're-distribution effect' on aerosol-cloud interaction and indirect radiative forcing.

5. Implication

This study highlights the impact of the 're-distribution effect' on moderating nitrate cooling and altering the nitrogen deposition efficiency by interacting with natural sea-salt aerosols (Fig. 1). A similar 're-distribution effect' may apply to the heterogeneous reaction and consumption of gaseous organic compounds, sulfuric and nitric acids on natural desert dust (Usher et al., 2003;Ponczek and George,

410   2018;Dupart et al., 2012;Ravishankara, 1997), although non-volatile particulate sulfate does not shift from fine to the coarse mode aerosols. Uptake of acids by dust particles can shorten their lifetimes and reduce their radiative forcing (Liao and Seinfeld, 2005;Harris et al., 2013;Karydis et al., 2016;Abdelkader et al., 2015), which could be significant over inland areas where sea-salt aerosol is lacking. All these previous studies imply the possibility that natural particles (sea-salt aerosol and very likely dust as well) moderate the

415   DRF of anthropogenic aerosols and alter the nitrogen and sulfur deposition efficiency. We highlight the importance of further study of the inter-actions between natural and anthropogenic aerosols. More comprehensive modelling studies with fully dynamic aerosol mass transfer treatment are needed for improving the assessment of aerosol climate effect accounting for the 're-distribution effect' on a global scale.

420

Acknowledgments

We would like to acknowledge the following funding resources: National Natural Science Foundation of China (91644218), the National Key R&D Program of China (2017YFC0210104) and Guangdong

425   Innovative and Entrepreneurial Research Team Program (2016ZT06N263). We thank Dr. Konrad Müller (TROPOS) for his contribution to the aerosol composition measurements. This work was supported by German Research Ministry (01LK1212C) and the Max Planck Society (MPG). Y. F. C. would also like to thank the Minerva Program of MPG.

Author contributions

430   Y. F. C. led the study. Y. F. C. and Y. C. conceived and design the study. Y. C. performed the WRF-Chem model simulations and processed the data. N. M. supported the optical calculation. C. W. supported the kinetic part of the model simulation and result analyses. A. P. and J. L. provided the EMAC global simulation. G. S. carried out the aerosol chemical composition observations at Melpitz. Y. C., Y. F. C. and H. S. interpreted the results. All co-authors discussed the results. Y. C. and Y. F. C. wrote the manuscript with

435   inputs from all co-authors.

Additional information

Correspondence and requests for materials should be addressed to and Y. F. C and Y. C.

Competing financial interests

The authors declare no competing financial interests.

Data availability

WRF-Chem model code and FINN fire emissions are openly available for download from the website www2.acom.ucar.edu. NCEP reanalysis data is openly available for download from the website https://rda.ucar.edu/. AERONET and aerosol observational datasets are openly available for download from the websites https://aeronet.gsfc.nasa.gov/ and http://ebas.nilu.no/default.aspx. The European emission inventory is available from AQMEII project (http://aqmeii.jrc.ec.europa.eu/) and EUCAARI project (https://www.atm.helsinki.fi/eucaari/?q=node/3). The global emission inventory is available from EDGAR project (http://edgar.jrc.ec.europa.eu). The results of EMAC global model is available from https://dx.doi.org/10.17635/lancaster/researchdata/297. All data needed to evaluate the conclusions in the paper are present in the paper and/or the Supporting Information. Additional data related to this paper should be addressed to and Y.F.C and Y.C.

References:

Abdelkader, M., Metzger, S., Mamouri, R. E., Astitha, M., Barrie, L., Levin, Z., and Lelieveld, J.: Dust–air pollution dynamics over the eastern Mediterranean, Atmos. Chem. Phys., 15, 9173-9189, 10.5194/acp-15-9173-2015, 2015.

Adams, P. J., Seinfeld, J. H., Koch, D., Mickley, L., and Jacob, D.: General circulation model assessment of direct radiative forcing by the sulfate-nitrate-ammonium-water inorganic aerosol system, Journal of Geophysical Research: Atmospheres, 106, 1097-1111, 10.1029/2000JD900512, 2001.

Archer-Nicholls, S., Lowe, D., Utembe, S., Allan, J., Zaveri, R. A., Fast, J. D., et al.: Gaseous chemistry and aerosol mechanism developments for version 3.5.1 of the online regional model, WRF-Chem. Geoscientific Model Development, 7, 2557–2579. https://doi.org/10.5194/gmd-7-2557-2014, 2014

Archer-Nicholls, S., Lowe, D., Lacey, F., Kumar, R., Xiao, Q., Liu, Y., Carter, E., Baumgartner, J., and Wiedinmyer, C.: Radiative Effects of Residential Sector Emissions in China: Sensitivity to Uncertainty in Black Carbon Emissions, Journal of Geophysical Research: Atmospheres, 124, 5029-5044, 10.1029/2018JD030120, 2019.

Bauer, S. E., Koch, D., Unger, N., Metzger, S. M., Shindell, D. T., and Streets, D. G.: Nitrate aerosols today and in 2030: a global simulation including aerosols and tropospheric ozone, Atmos. Chem. Phys., 7, 5043-5059, 10.5194/acp-7-5043-2007, 2007.

Bellouin, N., Rae, J., Jones, A., Johnson, C., Haywood, J., and Boucher, O.: Aerosol forcing in the Climate Model Intercomparison Project (CMIP5) simulations by HadGEM2-ES and the role of ammonium nitrate, Journal of Geophysical Research: Atmospheres, 116, D20206, 10.1029/2011JD016074, 2011.

Berner, A., and Luerzer, C.: Mass size distributions of traffic aerosols at Vienna, The Journal of Physical Chemistry, 84, 2079-2083, 10.1021/j100453a016, 1980.

Bertram, T. H., & Thornton, J. A.,Toward a general parameterization of N2O5 reactivity on aqueous particles: the competing effects of particle liquid water, nitrate and chloride. Atmospheric Chemistry and Physics, 9(4), 15181–15214. https://doi.org/doi:10.5194/acp-9-8351-2009, 2009.

Birmili, W., Wiedensohler, A., Heintzenberg, J., and Lehmann, K.: Atmospheric particle number size distribution in central Europe: Statistical relations to air masses and meteorology, Journal of Geophysical Research, 106, 32005-32018, DOI: 10.1029/2000JD000220, 2001.

Chen, Y., Zhao, C., Zhang, Q., Deng, Z. Z., Huang, M. Y., and Ma, X. C.: Aircraft study of mountain chimney effect of Beijing, china, Journal of Geophysical Research: Atmospheres, 114, 10.1029/2008JD010610, 2009.

Chen, Y., Cheng, Y., Ma, N., Wolke, R., Nordmann, S., Schüttauf, S., Ran, L., Wehner, B., Birmili, W., van der Gon, H. A. C. D., Mu, Q., Barthel, S., Spindler, G., Stieger, B., Müller, K., Zheng, G. J., Pöschl, U., Su, H., and Wiedensohler, A.: Sea salt emission, transport and influence on size-segregated nitrate simulation: a case study in northwestern Europe by WRF-Chem, Atmos. Chem. Phys., 16, 12081-12097, 10.5194/acp-16-12081-2016, 2016a.

Chen, Y., Cheng, Y. F., Nordmann, S., Birmili, W., Denier van der Gon, H. A. C., Ma, N., Wolke, R., Wehner, B., Sun, J., Spindler, G., Mu, Q., Pöschl, U., Su, H., and Wiedensohler, A.: Evaluation of the size segregation of elemental carbon (EC) emission in Europe: influence on the simulation of EC long-range transportation, Atmos. Chem. Phys., 16, 1823-1835, 10.5194/acp-16-1823-2016, 2016b.

Chen, Y., Wild, O., Wang, Y., Ran, L., Teich, M., Größ, J., Wang, L., Spindler, G., Herrmann, H., van Pinxteren, D., McFiggans, G., and Wiedensohler, A.: The influence of impactor size cut-off shift caused by hygroscopic growth on particulate matter loading and composition measurements, Atmospheric Environment, 195, 141-148, https://doi.org/10.1016/j.atmosenv.2018.09.049, 2018a.

Chen, Y., Wolke, R., Ran, L., Birmili, W., Spindler, G., Schröder, W., Su, H., Cheng, Y., Tegen, I., and Wiedensohler, A.: A parameterization of the heterogeneous hydrolysis of N2O5 for mass-based aerosol models: improvement of particulate nitrate prediction, Atmos. Chem. Phys., 18, 673-689, 10.5194/acp-18-673-2018, 2018b.

Chou, M.-D., Suarez, M. J., Ho, C.-H., Yan, M. M. H., and Lee, K.-T.: Parameterizations for Cloud Overlapping and Shortwave Single-Scattering Properties for Use in General Circulation and Cloud Ensemble Models, Journal of Climate, 11, 202-214, 10.1175/1520-0442(1998)011<0202:PFCOAS>2.0.CO;2, 1998.

Croft, B., Pierce, J. R., and Martin, R. V.: Interpreting aerosol lifetimes using the GEOS-Chem model and constraints from radionuclide measurements, Atmospheric Chemistry and Physics, 14, 4313-4325, 2014.

Ding, A., Wang, T., Zhao, M., Wang, T., and Li, Z.: Simulation of sea-land breezes and a discussion of their implications on the transport of air pollution during a multi-day ozone episode in the Pearl River Delta of China, Atmospheric Environment, 38, 6737-6750, https://doi.org/10.1016/j.atmosenv.2004.09.017, 2004.

Dupart, Y., King, S. M., Nekat, B., Nowak, A., Wiedensohler, A., Herrmann, H., David, G., Thomas, B., Miffre, A., Rairoux, P., D'Anna, B., and George, C.: Mineral dust photochemistry induces nucleation events in the presence of SO_2, Proceedings of the National Academy of Sciences, 109, 20842-20847, 10.1073/pnas.1212297109, 2012.

Fast, J. D., Gustafson Jr, W. I., Easter, R. C., Zaveri, R. A., Barnard, J. C., Chapman, E. G., Grell, G. A., and Peckham, S. E.: Evolution of ozone, particulates, and aerosol direct radiative forcing in the vicinity of Houston using a fully coupled meteorology-chemistry-aerosol model, Journal of Geophysical Research: Atmospheres, 111, 10.1029/2005JD006721, 2006.

Forster, P., Ramaswamy, V., Artaxo, P., Berntsen, T., Betts, R., Fahey, D. W., Haywood, J., Lean, J., Lowe, D. C., Myhre, G., Nganga, J., Prinn, R., Raga, G., Schulz, M., and Van Dorland, R.: Changes in Atmospheric Constituents and in Radiative Forcing, in: Climate Change 2007:The Physical Science Basis. Contribution of Working Group I to the Fourth Assessment Report of the Intergovernmental Panel on Climate Change, edited by: Solomon, S., Qin, D., Manning, M., Chen, Z., Marquis, M., Averyt, K. B., Tignor, M., and Miller, H. L., Cambridge University Press, Cambridge, United Kingdom and New York, NY, USA, 2007.

Gantt, B., Kelly, J. T., and Bash, J. O.: Updating sea spray aerosol emissions in the Community Multiscale Air Quality (CMAQ) model version 5.0.2, Geosci. Model Dev., 8, 3733-3746, 10.5194/gmd-8-3733-2015, 2015.

Gao, M., Ji, D., Liang, F., and Liu, Y.: Attribution of aerosol direct radiative forcing in China and India to emitting sectors, Atmospheric Environment, 190, 35-42, https://doi.org/10.1016/j.atmosenv.2018.07.011, 2018.

Gong, S. L.: A parameterization of sea-salt aerosol source function for sub- and super-micron particles, Global Biogeochemical Cycles, 17, 10.1029/2003GB002079, 2003.

Grell, G. A., Peckham, S. E., Schmitz, R., McKeen, S. A., Frost, G., Skamarock, W. C., and Eder, B.: Fully coupled "online" chemistry within the WRF model, Atmospheric Environment, 39, 6957-6975, http://dx.doi.org/10.1016/j.atmosenv.2005.04.027, 2005.

Gustafsson, M. E. R., and Franzén, L. G.: Inland transport of marine aerosols in southern Sweden, Atmospheric Environment, 34, 313-325, http://dx.doi.org/10.1016/S1352-2310(99)00198-3, 2000.

Harris, E., Sinha, B., van Pinxteren, D., Tilgner, A., Fomba, K. W., Schneider, J., Roth, A., Gnauk, T., Fahlbusch, B., Mertes, S., Lee, T., Collett, J., Foley, S., Borrmann, S., Hoppe, P., and Herrmann, H.: Enhanced Role of Transition Metal Ion Catalysis During In-Cloud Oxidation of SO2, Science, 340, 727-730, 10.1126/science.1230911, 2013.

Hauglustaine, D. A., Balkanski, Y., and Schulz, M.: A global model simulation of present and future nitrate aerosols and their direct radiative forcing of climate, Atmos. Chem. Phys., 14, 11031-11063, 10.5194/acp-14-11031-2014, 2014.

Haywood, J., and Schulz, M.: Causes of the reduction in uncertainty in the anthropogenic radiative forcing of climate between IPCC (2001) and IPCC (2007), Geophysical Research Letters, 34, L20701, 10.1029/2007GL030749, 2007.

Hong, S.-Y., Noh, Y., and Dudhia, J.: A new vertical diffusion package with an explicit treatment of entrainment processes, Mon. Weather Rev., 134, 2318-2341, 2006.

Huang, X., Song, Y., Zhao, C., Cai, X., Zhang, H., and Zhu, T.: Direct Radiative Effect by Multicomponent Aerosol over China, Journal of Climate, 28, 3472-3495, 10.1175/JCLI-D-14-00365.1, 2015.

IPCC: Climate Change 2013: The Physical Science Basis. Contribution of Working Group I to the Fifth Assessment Report of the Intergovernmental Panel on Climate Change, Report, edited by: Stocker, T. F., Qin D. H., Plattner, G. K., Tignor, M. M. B., Allen, S. K., Boschung, J., Nauels, A., Xia, Y., Bex, V., and Midgley, P. M.,, Cambridge University Press, New York, available at: http://www.ipcc.ch/report/ar5 (last access: 10 September, 2016), 2013.

Itahashi, S., Hayami, H., Uno, I., Pan, X., and Uematsu, M.: Importance of coarse-mode nitrate produced via sea salt as atmospheric input to East Asian oceans, Geophysical Research Letters, 10.1002/2016GL068722, 2016.

Jacobson, M. Z.: Global direct radiative forcing due to multicomponent anthropogenic and natural aerosols, Journal of Geophysical Research: Atmospheres, 106, 1551-1568, 10.1029/2000JD900514, 2001.

Jöckel, P., Kerkweg, A., Pozzer, A., Sander, R., Tost, H., Riede, H., Baumgaertner, A., Gromov, S., and Kern, B.: Development cycle 2 of the Modular Earth Submodel System (MESSy2), Geosci. Model Dev., 3, 717-752, 10.5194/gmd-3-717-2010, 2010.

Karydis, V. A., Tsimpidi, A. P., Pozzer, A., Astitha, M., and Lelieveld, J.: Effects of mineral dust on global atmospheric nitrate concentrations, Atmos. Chem. Phys., 16, 1491-1509, 10.5194/acp-16-1491-2016, 2016.

Klingmüller, K., Steil, B., Brühl, C., Tost, H., and Lelieveld, J.: Sensitivity of aerosol radiative effects to different mixing assumptions in the AEROPT 1.0 submodel of the EMAC atmospheric-chemistry–climate model, Geosci. Model Dev., 7, 2503-2516, 10.5194/gmd-7-2503-2014, 2014.

Köhler, H.: The nucleus in and the growth of hygroscopic droplets, Transactions of the Faraday Society, 32, 1152-1161, 10.1039/TF9363201152, 1936.

Kok, J. F., Ridley, D. A., Zhou, Q., Miller, R. L., Zhao, C., Heald, C. L., Ward, D. S., Albani, S., and Haustein, K.: Smaller desert dust cooling effect estimated from analysis of dust size and abundance, Nature Geosci, 10, 274-278, 10.1038/ngeo2912, 2017.

Kottek, M., Grieser, J., Beck, C., Rudolf, B., and Rubel, F.: World Map of the Köppen-Geiger climate classification updated, Meteorologische Zeitschrift, 15, 259-263, 10.1127/0941-2948/2006/0130, 2006.

Kulmala, M., Asmi, A., Lappalainen, H. K., Baltensperger, U., Brenguier, J. L., Facchini, M. C., Hansson, H. C., Hov, Ø., O'Dowd, C. D., Pöschl, U., Wiedensohler, A., Boers, R., Boucher, O., de Leeuw, G., Denier van der Gon, H. A. C., Feichter, J., Krejci, R., Laj, P., Lihavainen, H., Lohmann, U., McFiggans, G., Mentel, T., Pilinis, C., Riipinen, I., Schulz, M., Stohl, A., Swietlicki, E., Vignati, E., Alves, C., Amann, M., Ammann, M., Arabas, S., Artaxo, P., Baars, H., Beddows, D. C. S., Bergström, R., Beukes, J. P., Bilde, M., Burkhart, J. F., Canonaco, F., Clegg, S. L., Coe, H., Crumeyrolle, S., D'Anna, B., Decesari, S., Gilardoni, S., Fischer, M., Fjaeraa, A. M., Fountoukis, C., George, C., Gomes, L., Halloran, P., Hamburger, T., Harrison, R. M., Herrmann, H., Hoffmann, T., Hoose, C., Hu, M., Hyvärinen, A., Hõrrak, U., Iinuma, Y., Iversen, T., Josipovic, M., Kanakidou, M., Kiendler-Scharr, A., Kirkevåg, A., Kiss, G., Klimont, Z., Kolmonen, P., Komppula, M., Kristjánsson, J. E., Laakso, L., Laaksonen, A., Labonnote, L., Lanz, V. A., Lehtinen, K. E. J., Rizzo, L. V., Makkonen, R., Manninen, H. E., McMeeking, G., Merikanto, J., Minikin, A., Mirme, S., Morgan, W. T., Nemitz, E., O'Donnell, D., Panwar, T. S., Pawlowska, H., Petzold, A., Pienaar, J. J., Pio, C., Plass-Duelmer, C., Prévôt, A. S. H., Pryor, S., Reddington, C. L., Roberts, G., Rosenfeld, D., Schwarz, J., Seland, Ø., Sellegri, K., Shen, X. J., Shiraiwa, M., Siebert, H., Sierau, B., Simpson, D., Sun, J. Y., Topping, D., Tunved, P., Vaattovaara, P., Vakkari, V., Veefkind, J. P., Visschedijk, A., Vuollekoski, H., Vuolo, R., Wehner, B., Wildt, J., Woodward, S., Worsnop, D. R., van Zadelhoff, G. J., Zardini, A. A., Zhang, K., van Zyl, P. G., Kerminen, V. M., S Carslaw, K., and Pandis, S. N.: General overview: European Integrated project on Aerosol Cloud Climate and Air Quality interactions (EUCAARI) – integrating aerosol research from nano to global scales, Atmos. Chem. Phys., 11, 13061-13143, 10.5194/acp-11-13061-2011, 2011.

Li, S., Garay, M. J., Chen, L., Rees, E., and Liu, Y.: Comparison of GEOS-Chem aerosol optical depth with AERONET and MISR data over the contiguous United States, Journal of Geophysical Research: Atmospheres, 118, 11,228-211,241, 10.1002/jgrd.50867, 2013.

Liao, H., Seinfeld, J. H., Adams, P. J., and Mickley, L. J.: Global radiative forcing of coupled tropospheric ozone and aerosols in a unified general circulation model, Journal of Geophysical Research: Atmospheres, 109, D16207, 10.1029/2003JD004456, 2004.

Liao, H., and Seinfeld, J. H.: Global impacts of gas-phase chemistry-aerosol interactions on direct radiative forcing by anthropogenic aerosols and ozone, Journal of Geophysical Research: Atmospheres, 110, D18208, 10.1029/2005JD005907, 2005.

Lin, Y., Farley, R., and Orville, H.: Bulk Parameterization of the Snow Field in a Cloud Model, J. Clim. Appl. Meteorol., 22, 1065-1092, 1983.

Lowe, D., Archer-Nicholls, S., Morgan, W., Allan, J., Utembe, S., Ouyang, B., Aruffo, E., Le Breton, M., Zaveri, R. A., Di Carlo, P., Percival, C., Coe, H., Jones, R., and McFiggans, G.: WRF-Chem model predictions of the regional impacts of N2O5 heterogeneous processes on night-time chemistry over north-western Europe, Atmos. Chem. Phys., 15, 1385-1409, 10.5194/acp-15-1385-2015, 2015.

Macke, A., Seifert, P., Baars, H., Barthlott, C., Beekmans, C., Behrendt, A., Bohn, B., Brueck, M., Bühl, J., Crewell, S., Damian, T., Deneke, H., Düsing, S., Foth, A., Di Girolamo, P., Hammann, E., Heinze, R., Hirsikko, A., Kalisch, J., Kalthoff, N., Kinne, S., Kohler, M., Löhnert, U., Madhavan, B. L., Maurer, V., Muppa, S. K., Schween, J., Serikov, I., Siebert, H., Simmer, C., Späth, F., Steinke, S., Träumner, K., Trömel, S., Wehner, B., Wieser, A., Wulfmeyer, V., and Xie, X.: The HD(CP)2 Observational Prototype Experiment (HOPE) – an overview, Atmos. Chem. Phys., 17, 4887-4914, 10.5194/acp-17-4887-2017, 2017.

May, N. W., Gunsch, M. J., Olson, N., Bondy, A. L., Kirpes, R. M., Bertman, S., China, S., Laskin, A., Hopke, P. K., Ault, A. P., and Pratt, K. A.: Unexpected contributions of sea spray and lake spray aerosol to inland particulate matter, Environmental Science & Technology Letters, 10.1021/acs.estlett.8b00254, 2018.

Murphy, D. M., Anderson, J. R., Quinn, P. K., McInnes, L. M., Brechtel, F. J., Kreidenweis, S. M., Middlebrook, A. M., Posfai, M., Thomson, D. S., and Buseck, P. R.: Influence of sea-salt on aerosol radiative properties in the Southern Ocean marine boundary layer, Nature, 392, 62-65, 1998.

Myhre, G., Grini, A., and Metzger, S.: Modelling of nitrate and ammonium-containing aerosols in presence of sea salt, Atmos. Chem. Phys., 6, 4809-4821, 10.5194/acp-6-4809-2006, 2006.

Myhre, G., Samset, B. H., Schulz, M., Balkanski, Y., Bauer, S., Berntsen, T. K., Bian, H., Bellouin, N., Chin, M., Diehl, T., Easter, R. C., Feichter, J., Ghan, S. J., Hauglustaine, D., Iversen, T., Kinne, S., Kirkevåg, A., Lamarque, J. F., Lin, G., Liu, X., Lund, M. T., Luo, G., Ma, X., van Noije, T., Penner, J. E., Rasch, P. J., Ruiz, A., Seland, Ø., Skeie, R. B., Stier, P., Takemura, T., Tsigaridis, K., Wang, P., Wang, Z., Xu, L., Yu, H., Yu, F., Yoon, J. H., Zhang, K., Zhang, H., and Zhou, C.: Radiative forcing of the direct aerosol effect from AeroCom Phase II simulations, Atmos. Chem. Phys., 13, 1853-1877, 10.5194/acp-13-1853-2013, 2013.

Neumann, D., Matthias, V., Bieser, J., Aulinger, A., and Quante, M.: A comparison of sea salt emission parameterizations in northwestern Europe using a chemistry transport model setup, Atmos. Chem. Phys., 16, 9905-9933, 10.5194/acp-16-9905-2016, 2016.

Neusüß, C., Weise, D., Birmili, W., Wex, H., Wiedensohler, A., and Covert, D. S.: Size-segregated chemical, gravimetric and number distribution-derived mass closure of the aerosol in Sagres, Portugal during ACE-2, Tellus B, 52, 169-184, 10.1034/j.1600-0889.2000.00039.x, 2000.

O'Dowd, C. D., Smith, M. H., Consterdine, I. E., and Lowe, J. A.: Marine aerosol, sea-salt, and the marine sulphur cycle: a short review, Atmospheric Environment, 31, 73-80, http://dx.doi.org/10.1016/S1352-2310(96)00106-9, 1997.

Petters, M. D., and Kreidenweis, S. M.: A single parameter representation of hygroscopic growth and cloud condensation nucleus activity, Atmos. Chem. Phys., 7, 1961-1971, 10.5194/acp-7-1961-2007, 2007.

Ponczek, M., and George, C.: Kinetics and Product Formation during the Photooxidation of Butanol on Atmospheric Mineral Dust, Environmental Science & Technology, 52, 5191-5198, 10.1021/acs.est.7b06306, 2018.

Pouliot, G., Pierce, T., Denier van der Gon, H., Schaap, M., Moran, M., and Nopmongcol, U.: Comparing emission inventories and model-ready emission datasets between Europe and North America for the AQMEII project, Atmospheric Environment, 53, 4-14, http://dx.doi.org/10.1016/j.atmosenv.2011.12.041, 2012.

Pozzer, A., de Meij, A., Pringle, K. J., Tost, H., Doering, U. M., van Aardenne, J., and Lelieveld, J.: Distributions and regional budgets of aerosols and their precursors simulated with the EMAC chemistry-climate model, Atmos. Chem. Phys., 12, 961-987, 10.5194/acp-12-961-2012, 2012.

Pringle, K. J., Tost, H., Message, S., Steil, B., Giannadaki, D., Nenes, A., Fountoukis, C., Stier, P., Vignati, E., and Lelieveld, J.: Description and evaluation of GMXe: a new aerosol submodel for global simulations (v1), Geosci. Model Dev., 3, 391-412, 10.5194/gmd-3-391-2010, 2010.

Ravishankara, A. R.: Heterogeneous and Multiphase Chemistry in the Troposphere, Science, 276, 1058-1065, 10.1126/science.276.5315.1058, 1997.

Saide, P. E., Spak, S. N., Carmichael, G. R., Mena-Carrasco, M. A., Yang, Q., Howell, S., Leon, D. C.,

Snider, J. R., Bandy, A. R., Collett, J. L., Benedict, K. B., de Szoeke, S. P., Hawkins, L. N., Allen, G., Crawford, I., Crosier, J., and Springston, S. R.: Evaluating WRF-Chem aerosol indirect effects in Southeast Pacific marine stratocumulus during VOCALS-REx, Atmos. Chem. Phys., 12, 3045-3064, 10.5194/acp-12-3045-2012, 2012.

Seinfeld, J. H., and Pandis, S. N.: Atmospheric Chemistry and Physics: From Air Pollution to Climate Change, John Wiley & Sons, New York, 2nd Edn., 2006.

Spindler, G., Gnauk, T., Grüner, A., Iinuma, Y., Müller, K., Scheinhardt, S., and Herrmann, H.: Size-segregated characterization of PM10 at the EMEP site Melpitz (Germany) using a five-stage impactor: a six year study, J Atmos Chem, 69, 127-157, 10.1007/s10874-012-9233-6, 2012.

Streets, D. G., Shindell, D. T., Lu, Z., and Faluvegi, G.: Radiative forcing due to major aerosol emitting sectors in China and India, Geophysical Research Letters, 40, 4409-4414, 10.1002/grl.50805, 2013.

Usher, C. R., Michel, A. E., and Grassian, V. H.: Reactions on Mineral Dust, Chemical Reviews, 103, 4883-4940, 10.1021/cr020657y, 2003.

van Dorland, R., Dentener, F. J., and Lelieveld, J.: Radiative forcing due to tropospheric ozone and sulfate aerosols, Journal of Geophysical Research: Atmospheres, 102, 28079-28100, 10.1029/97JD02499, 1997.

Vivanco, M. G., Bessagnet, B., Cuvelier, C., Theobald, M. R., Tsyro, S., Pirovano, G., Aulinger, A., Bieser, J., Calori, G., Ciarelli, G., Manders, A., Mircea, M., Aksoyoglu, S., Briganti, G., Cappelletti, A., Colette, A., Couvidat, F., D'Isidoro, M., Kranenburg, R., Meleux, F., Menut, L., Pay, M. T., Rouïl, L., Silibello, C., Thunis, P., and Ung, A.: Joint analysis of deposition fluxes and atmospheric concentrations of inorganic nitrogen and sulphur compounds predicted by six chemistry transport models in the frame of the EURODELTAIII project, Atmospheric Environment, 151, 152-175, https://doi.org/10.1016/j.atmosenv.2016.11.042, 2017.

Wang, Y., and Chen, Y.: Significant Climate Impact of Highly Hygroscopic Atmospheric Aerosols in Delhi, India, Geophysical Research Letters, 0, 10.1029/2019GL082339, 2019.

Wild, O., Zhu, X., and Prather, M. J.: Fast-J: Accurate Simulation of In- and Below-Cloud Photolysis in Tropospheric Chemical Models, J. Atmos. Chem., 37, 245-282, 2000.

Xu, L., and Penner, J. E.: Global simulations of nitrate and ammonium aerosols and their radiative effects, Atmos. Chem. Phys., 12, 9479-9504, 10.5194/acp-12-9479-2012, 2012.

Yao, H., Song, Y., Liu, M., Archer-Nicholls, S., Lowe, D., McFiggans, G., Xu, T., Du, P., Li, J., Wu, Y., Hu, M., Zhao, C., and Zhu, T.: Direct radiative effect of carbonaceous aerosols from crop residue burning during the summer harvest season in East China, Atmos. Chem. Phys., 17, 5205-5219, 10.5194/acp-17-5205-2017, 2017.

Zaveri, R. A., and Peters, L. K.: A new lumped structure photochemical mechanism for large-scale applications, J. Geophys. Res., 104, 30387-30415, 1999.

Zaveri, R. A., Easter, R. C., Fast, J. D., and Peters, L. K.: Model for Simulating Aerosol Interactions and Chemistry (MOSAIC), Journal of Geophysical Research: Atmospheres, 113, 10.1029/2007JD008782, 2008.

Table 1. Configurations of WRF-Chem

Physics	WRF options
Micro physics	Lin scheme (Lin, 1983)
Boundary layer	YSU (Hong, 2006)
Surface	Rapid Update Cycle (RUC) land surface model
Shortwave radiation	Goddard shortwave (Chou et al., 1998)
Longwave radiation	New Goddard scheme
Cumulus	Grell 3D
Urban	3-category UCM
Chemistry and Aerosol	**Chem options**
Aerosol module	MOSAIC with 8 bins (Zaveri et al., 2008)
Gas-phase mechanism	CBMZ (Zaveri and Peters, 1999)
Photolytic rate	Fast-J photolysis scheme (Wild et al., 2000)
Sea salt emission	Gong scheme (Gong, 2003)
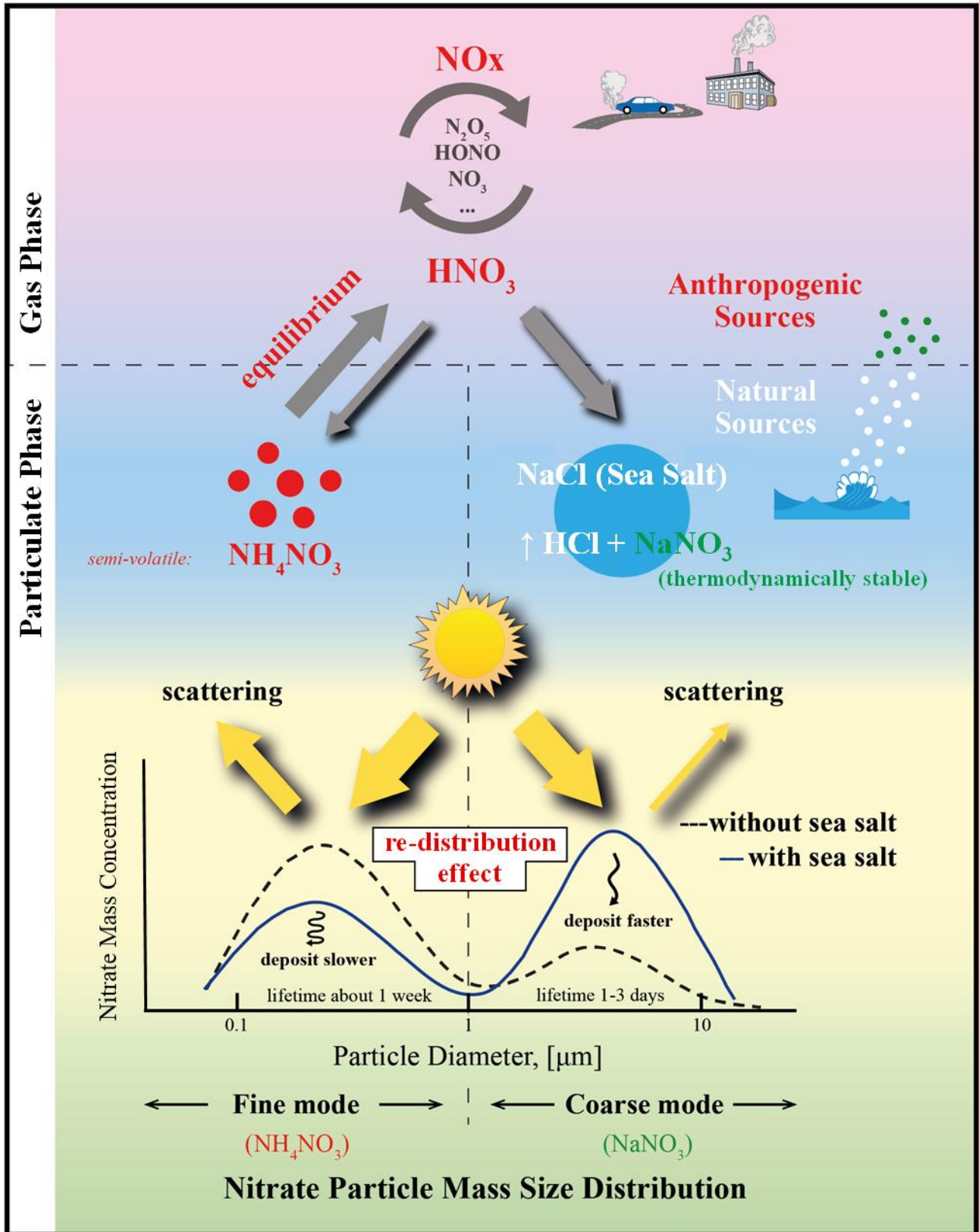
Fig. 1. Concept of the sea-salt aerosol induced 're-distribution effect'.
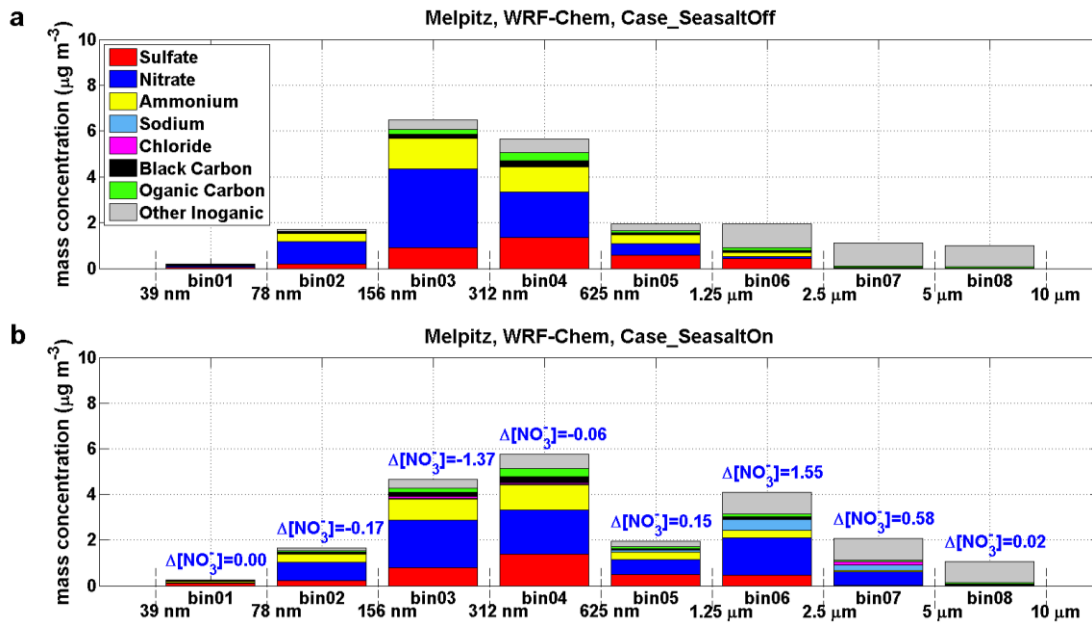
Fig. 2. Model results of mass concentration of each chemical compounds in eight size bins at Melpitz.
The results showed here are averaged during 17 September 2013 when marine air masses started
approaching Melpitz. Sodium is used as an indicator of sea-salt aerosol. **a**, Result of the 'Case_SeasaltOff'
(without sea-salt emission). **b**, Result of the 'Case_SeasaltOn' (with sea-salt emission). The differences
of particulate nitrate mass concentration ($\Delta[NO_3^-]$) in each size bin are marked.
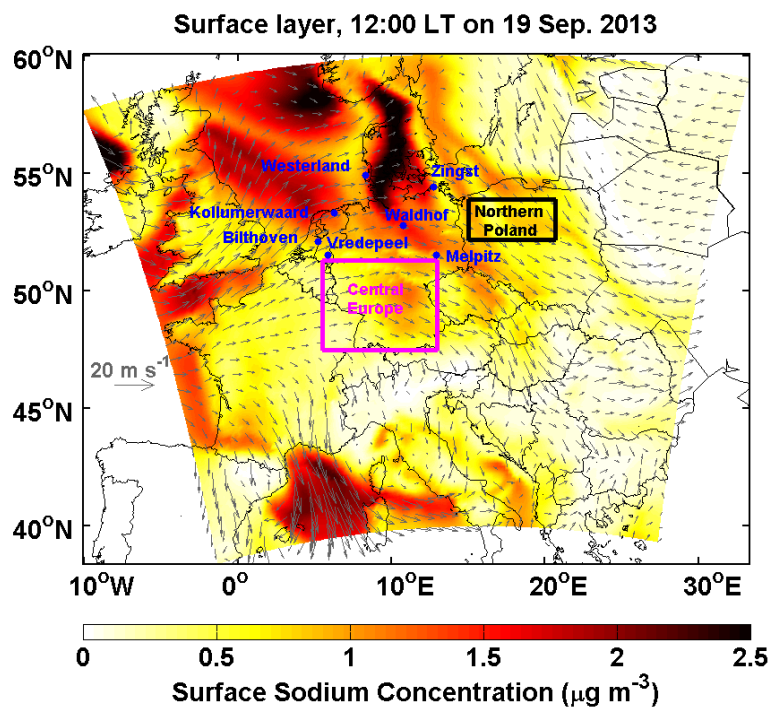
**Fig. 3. Surface sodium mass concentration over Europe domain at 12:00 local time (LT) on 19 September
2013.** The 10-meter wind is indicated by the grey arrows. The results are based on the 'Case_SeasaltOn'. Westerland,
Waldhof, Zingst, Bilthoven, Kollumerwaard, Vredepeel, Melpitz, Central Europe and the northern Poland regions
are marked.
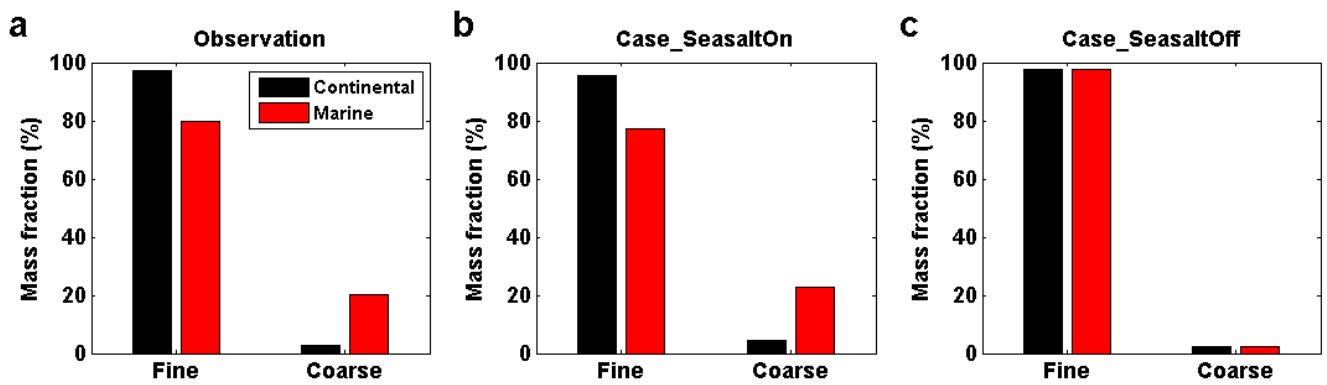
Fig. 4. Observed and simulated mass fraction of particulate nitrate in fine and coarse modes at Melpitz, Germany. **a**, Observation based on the Berner impactor measurements. **b**, WRF-Chem 'Case_SeasaltOn' simulation, i.e., with sea-salt emission. **c**, WRF-Chem 'Case_SeasaltOff' simulation, i.e., without sea-salt emission. The results are grouped into continental (black bar) and marine (red bar) air mass types, respectively. According to the size-cuts of the Berner impactor, the size ranges of the fine and coarse mode particles are defined as $PM_{1.2}$ (particles with an aerodynamic diameter smaller than 1.2 μm) and $PM_{1.2-10}$ (particles with an aerodynamic diameter larger than 1.2 μm and smaller than 10 μm), respectively.
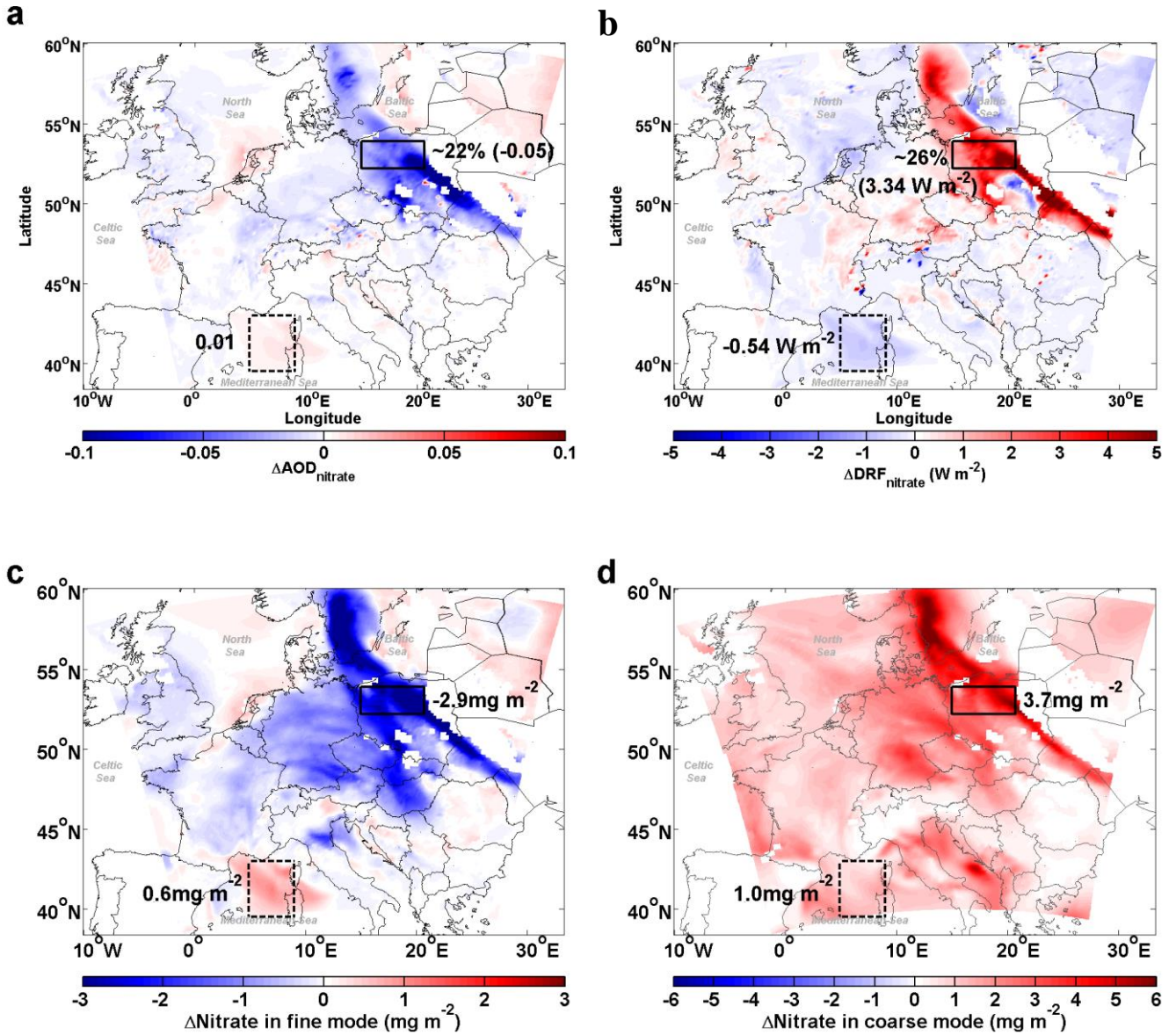
Fig. 5. Influence of sea-salt on the abundance and direct radiative forcing of nitrate. Differences ('Case_SeasaltOn' – 'Case_SeasaltOff') between simulations with and without sea-salt emission in aerosol optical depth ($\Delta AOD_{nitrate}$, **a**), direct radiative forcing ($\Delta DRF_{nitrate}$, **b**), and column loading of nitrate ($\Delta Nitrate$) for the fine (**c**) and coarse (**d**) mode particles, during daytime, i.e., 07:00-16:00 local time (LT) on 19 September 2013. The northern Poland and Mediterranean regions are marked by boxes with solid and dashed black frames, respectively.
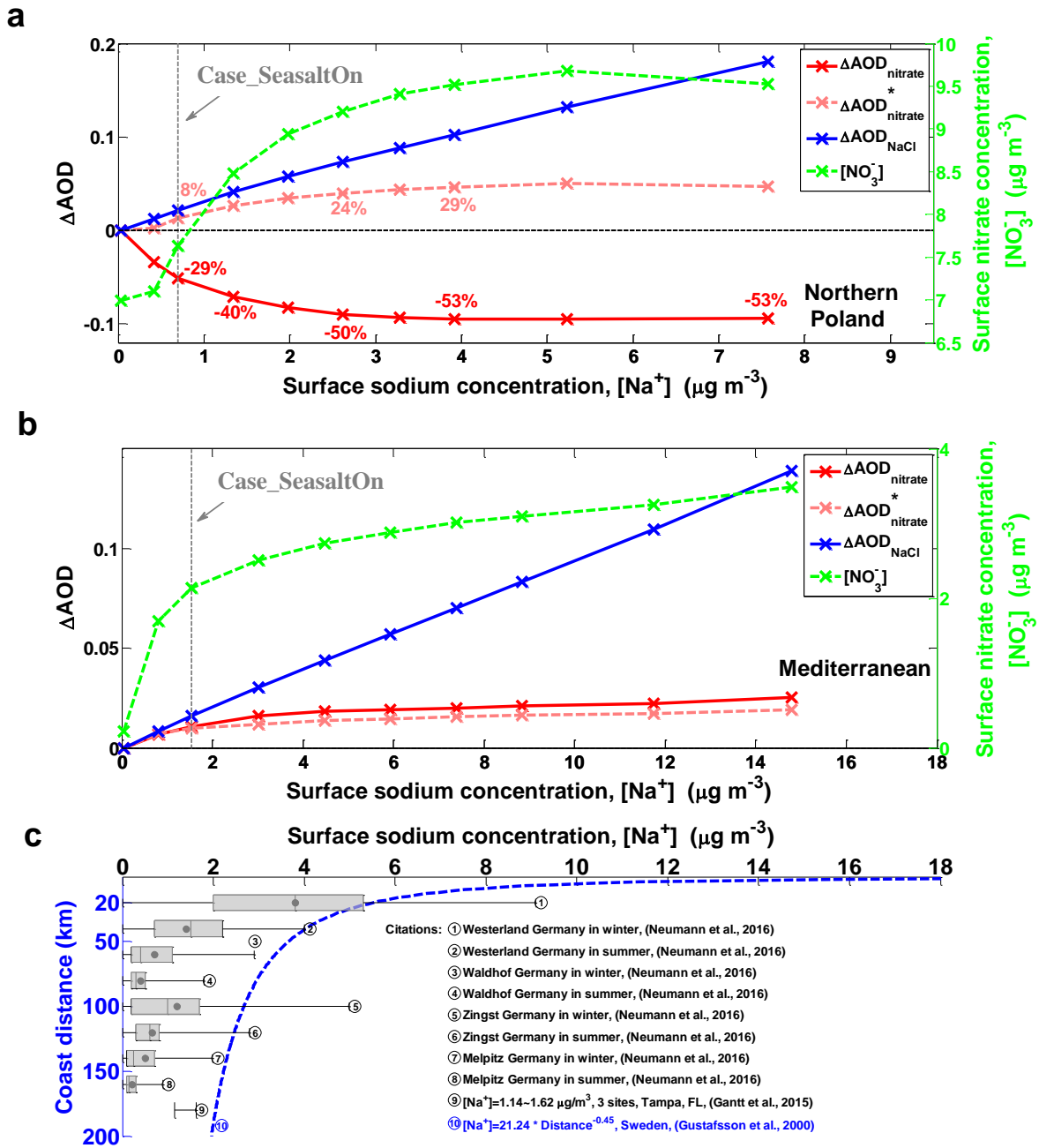
Fig. 6. Sensitivity of aerosol optical depth (ΔAOD) as a function of sodium mass concentration ([Na⁺]). Differences between the 'Case_SeasaltOff' and sensitivity cases (sea-salt emission with different scaling factors) for different aerosol components, i.e., nitrate (ΔAOD$_{nitrate}$) and sea-salt (ΔAOD$_{NaCl}$): ΔAOD (sensitivity case – 'Case_SeasaltOff') versus [Na⁺] over northern Poland (**a**) and Mediterranean regions (**b**), respectively. The model results shown here are averages over a sea-salt event during daytime (07:00-16:00 LT) on 19 September 2013. The results of surface [NO$_3^-$] are indicated by the green dashed line. Here, the 'Case_SeasaltOff' is the reference case and the 'Case_SeasaltOn' is marked. Note: ΔAOD$^*_{nitrate}$ (pink dashed line) indicates the ΔAOD of nitrate calculated by re-allocating nitrate mass into different size bins according to the normalized nitrate particle mass size distribution simulated in 'Case_SeasaltOff' (i.e., without 're-distribution effect'). **c,** The measured [Na⁺] at different sites over Sweden as a function of coast distance, and in Germany (marked in Fig. 3) and US. The box-whisker plots of the references ①-⑧ indicate the median, mean (black dot), 25% percentile, 75% percentile, maximum and minimum. The error bar of the reference ⑨ indicates the range. The blue dashed line of the reference ⑩ indicates the statistically empirical function of [Na⁺] with the distance from coast, based on the network measurements of 16 sites in Sweden.
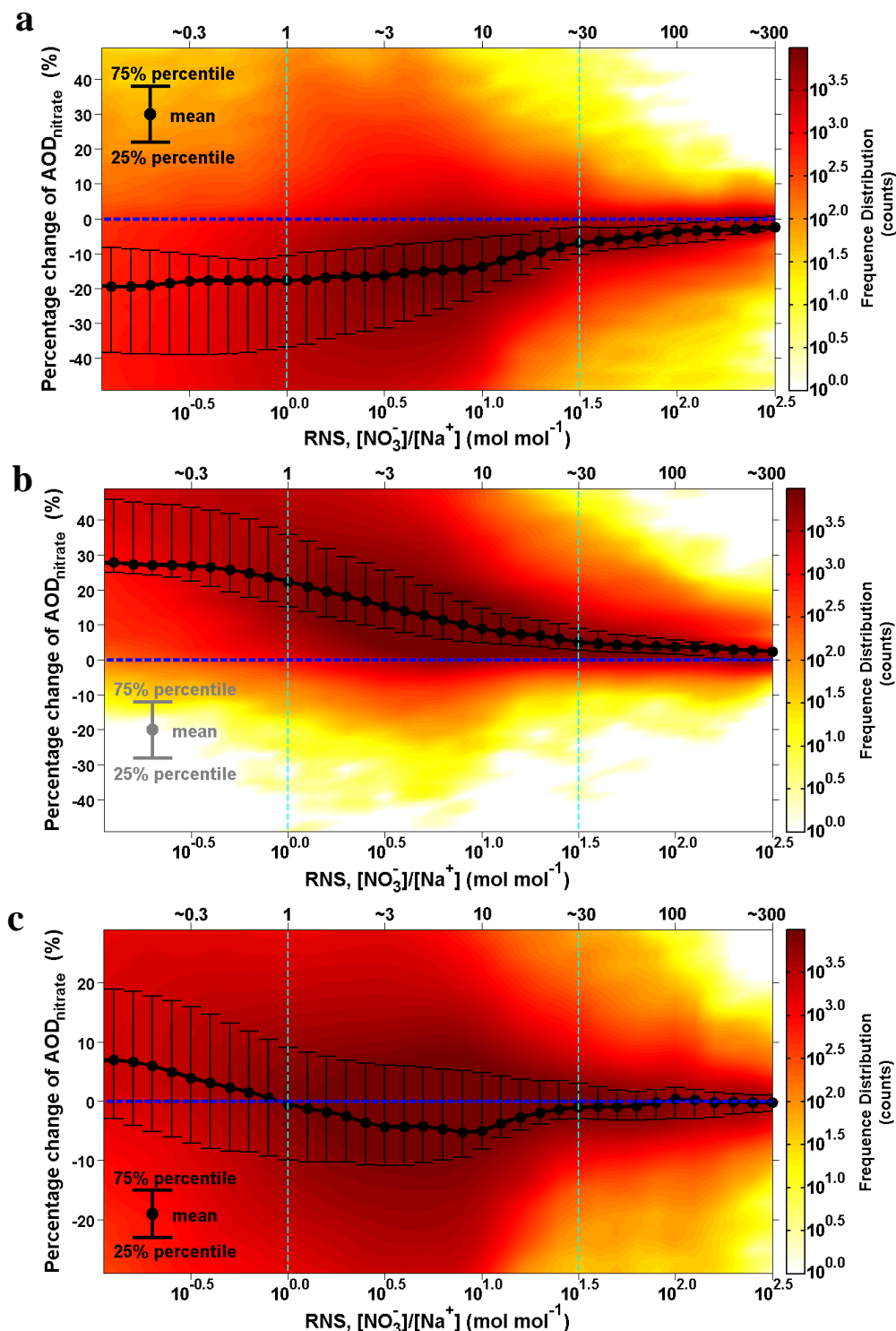
Fig. 7. Intensity of 're-distribution effect' as a function of molar ratio between surface fine nitrate and total sodium (RNS) over European domain. (a) The intensity of the 're-distribution effect' is calculated as the difference in percentage between $AOD_{nitrate}$ and $AOD^*_{nitrate}$ in the 'Case_SeasaltOn'; **(b)** the intensity of 'mass-enhancement effect'. The black dots indicate the mean values; the upper and lower error bars indicate the 75% and 25% percentile, respectively; and **(c)** the net effect of 'mass-enhancement' and 're-distribution';The colour indicates the frequency distribution (i.e., how many counts) of the hourly model results over entire Europe domain during 16-20 September 2013. The coverage of model results between the two light blue dashed lines is ~70%.
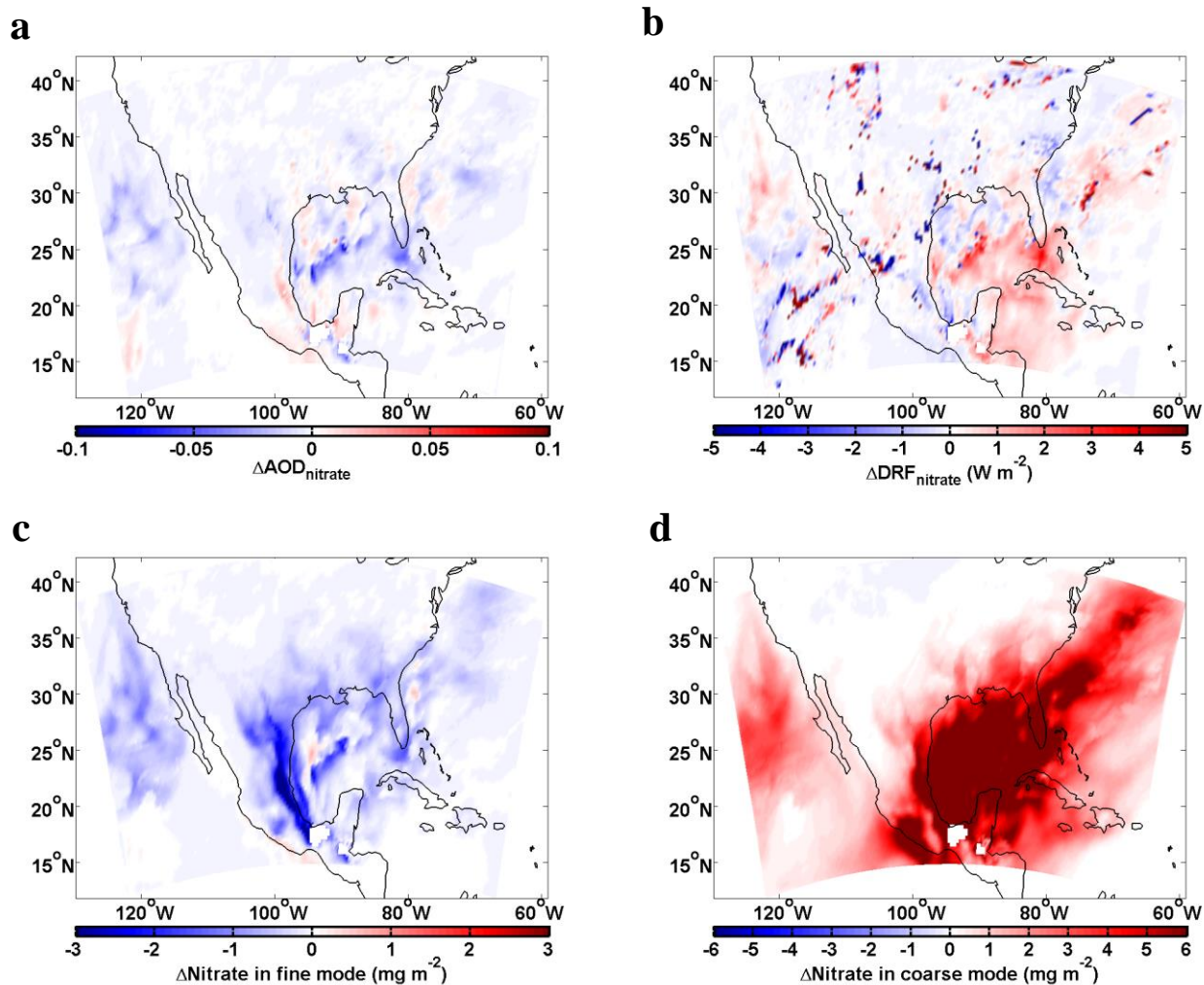
Fig. 8. Influence of sea-salt aerosol on the abundance and direct radiative forcing of nitrate (similar as Fig. 5). Differences ('Case_SeasaltOn' – 'Case_SeasaltOff') between simulations with and without sea-salt emission in aerosol optical depth ($\Delta AOD_{nitrate}$, **a**), direct radiative forcing ($\Delta DRF_{nitrate}$, **b**), and column loading of nitrate ($\Delta Nitrate$) for the fine (**c**) and coarse (**d**) mode particles. The modelled results showed here are averaged during daytime over North America domain, i.e., 16:00-22:00 (UTC) on 10-17 January 2015.
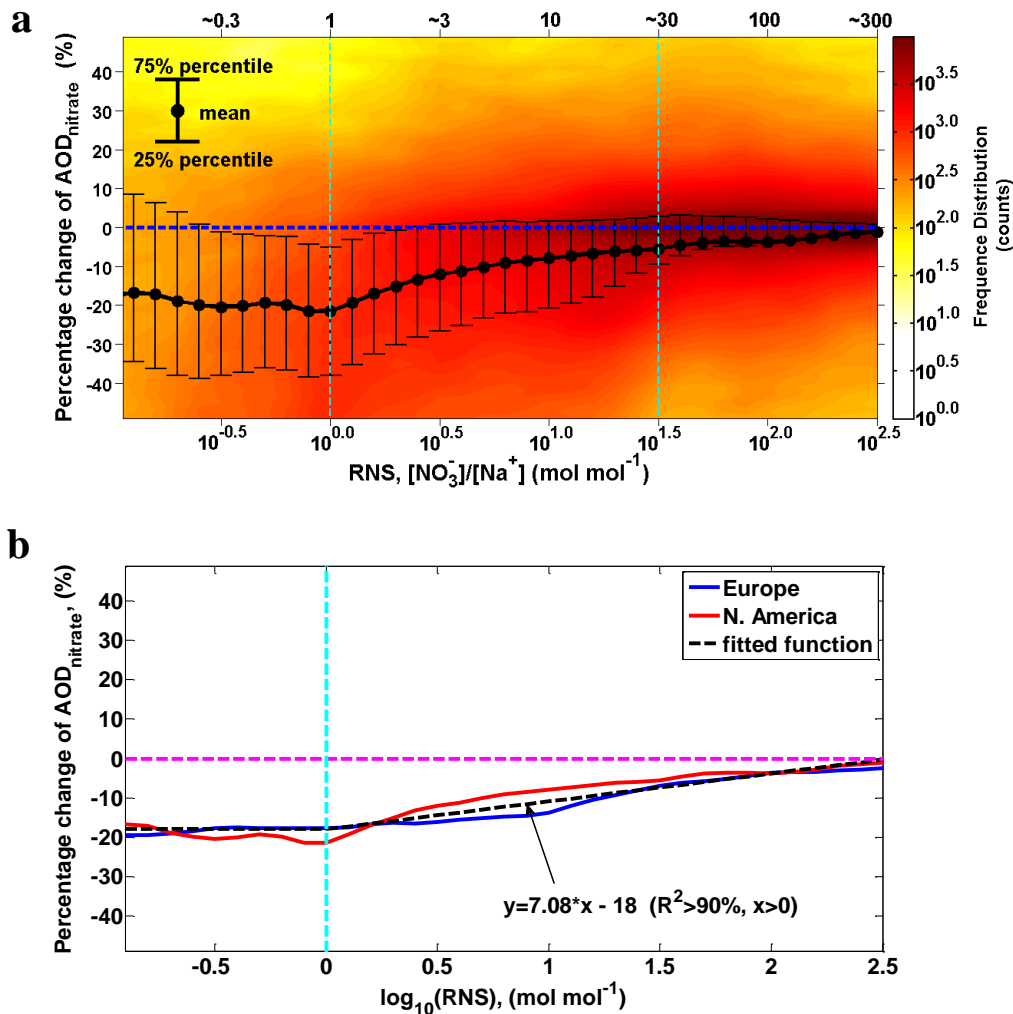
Fig. 9. Intensity of 're-distribution effect' as a function of molar ratio between surface fine nitrate and total sodium (RNS). **(a)** The intensity of 're-distribution effect' over North American domain, similar as Fig. 7a, calculated as the difference in percentage between $AOD_{nitrate}$ and $AOD^*_{nitrate}$ in the 'Case_SeasaltOn'. $AOD^*_{nitrate}$ indicates the $AOD_{nitrate}$ calculated by re-allocating nitrate mass into different size bins according to the normalized nitrate particle mass size distribution simulated in 'Case_SeasaltOff' (i.e., without 're-distribution effect'). The black dots indicate the mean values; the upper and lower error bars indicate the 75% and 25% percentile, respectively. The colour indicates the frequency distribution (i.e., how many counts) of the hourly model results over entire North America domain during 10-17 January 2015. **(b)** The median possibility of the percentage change of $AOD_{nitrate}$ as a function (first-order approximation) of RNS.
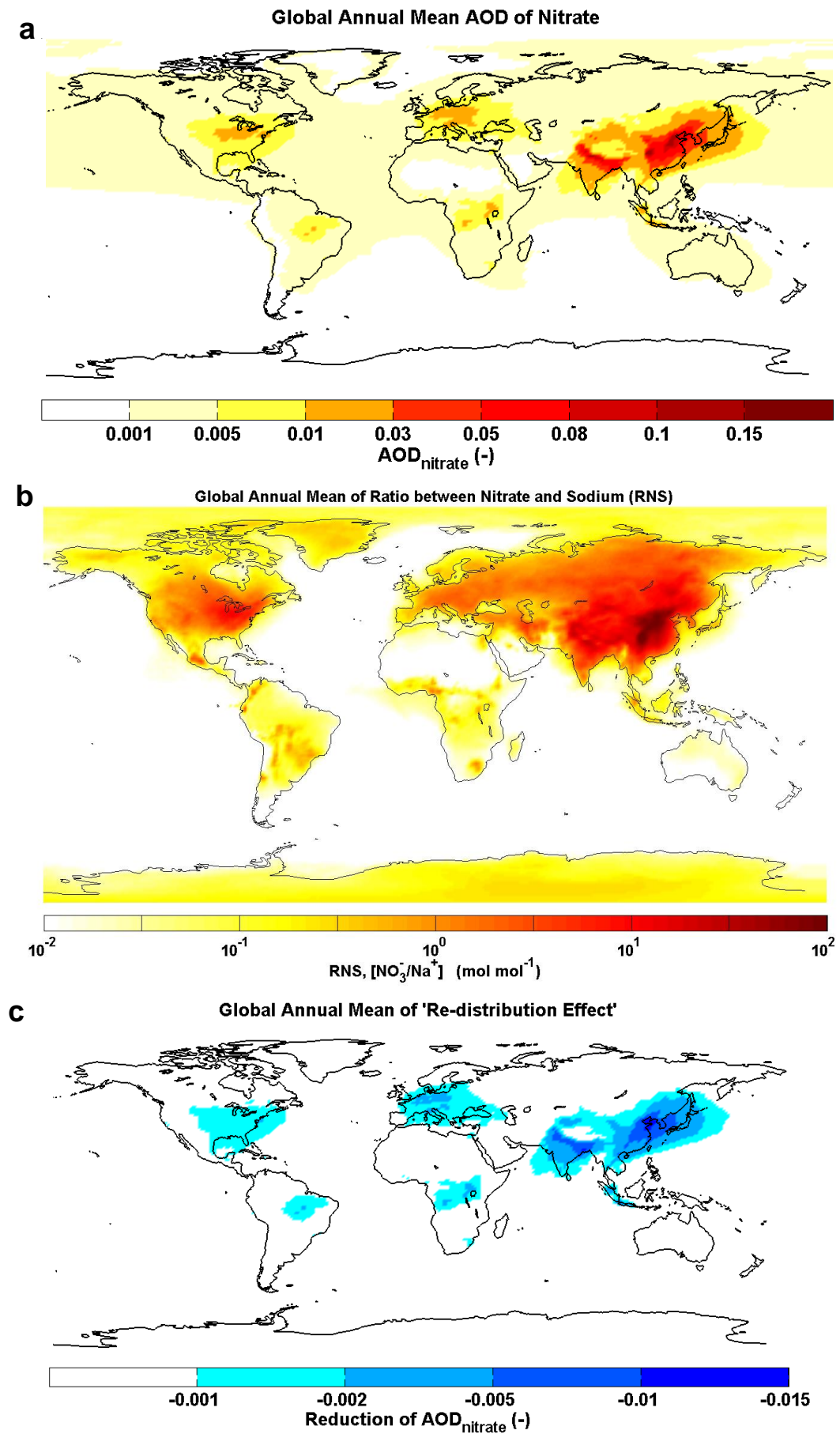
Fig. 10. The global distribution of annual mean AOD$_{nitrate}$ (a), RNS (b) and reduction of AOD$_{nitrate}$ associated with the 'Re-distribution effect' (c). The results of (a, b) are simulated with the EMAC model, the results of (c) are estimated from the first-order approximation in Fig. 9b.